jonathan mcDowell
1982 Aug.

Relativistically Beamed Quasi-Stellar Objects

1. The model to be tested

The suggestion by Browne et al (1982) within the framework of the relativistic jet model of radio sources that compact radio quasars are just classical double radio quasars seen end on, with relativistic beaming of the central component, is analysed using a sample of 3CR quasars. Non-quasars are not considered in this study.

In our specific model 2 opposed relativistic jets of Lorentz factor γ make up the central component of the source with intrinsic luminosity P_o, observed luminosity $P_c = P_c(P_o, \gamma, \theta)$ where θ is the angle between the axis of the source and the line of sight. The extended structure has the same axis and is unbeamed with luminosity P_e. The source has physical size D, and projected size $cl = D \sin\theta$.

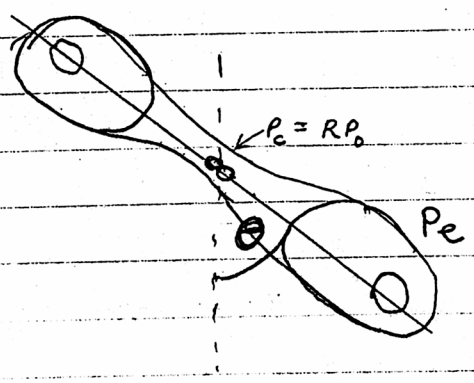

The observable quantities are $S(\nu)$ (the flux density at frequency ν) ϕ, the angular diameter, $\alpha(\nu)$ (the spectral index) and z, the redshift of the quasar. These quantities are related as follows:

Define $D_L = \left(\frac{c}{H_o}\right) \frac{2[\Omega z + (\Omega - 2)(\sqrt{1+\Omega z} - 1)]}{\Omega^2 (1+z)}$, the luminosity distance

Then $d = \frac{\phi D_L}{1+z}$

$$P_c = S_c D_L^2 (1+z)^{1+\alpha_c}$$

$$P_e = S_e D_L^2 (1+z)^{1+\alpha_e}$$

where the subscripts e and c refer to the extended and central components of the source throughout.

Typically we expect $\alpha_c \approx 0$ $\alpha_e \sim 0.8$

Now the relation between P_e and P_o is given by the sum of the beaming factors for each of the twin beams;

$$R = \frac{1}{\gamma^3(1-\beta\cos\theta)^3}$$ for one beam, $(\alpha_c \approx 0)$

$\beta = v/c = \sqrt{1-1/\gamma^2}$

so for our model

$$R(\gamma,\theta) \equiv \frac{P_c}{P_o} = \frac{1}{2\gamma^3(1-\beta\cos\theta)^3} + \frac{1}{2\gamma^3(1+\beta\cos\theta)^3}$$ the beaming ratio

We only know

$$R_{obs} \equiv \frac{P_c}{P_e}$$ the flux ratio (luminosity)

but we may define the (orientation-independent) quantity λ, the intrinsic flux ratio, as

$$\lambda \equiv \frac{P_e}{P_o} = \frac{\text{Luminosity in extended components}}{\text{Intrinsic (unbeamed) luminosity of central component}}$$

Thus

$$R_{obs} = \frac{1}{2\gamma^3\lambda}\left[\frac{1}{(1-\beta\cos\theta)^3} + \frac{1}{(1+\beta\cos\theta)^3}\right]$$

So our model has two parameters, γ and λ, which, once chosen, give the angle to the line of sight from the observed flux ratio R_{obs}.

We must assume that the sources are randomly oriented in space; their projected angles to the line of sight θ will then be distributed as $\sin\theta\, d\theta = -d(\cos\theta)$; thus equal intervals of $\cos\theta$ should contain equal numbers of sources, and so $\cos\theta$ is the appropriate variable to use as an ordinate.

2. The sample

The quasars to be studied have been selected for their radio flux at 178 MHz; they are chosen from the Laing, Riley and Longair (1982) sample of radio sources with $S_{178} \geq 10$ Jy, $\delta \geq 10°$ and $|b| \geq 10°$, based on the 3CR catalogue. The sample comprises 43 quasars, subdivided into 14 compact quasars, 6 classical doubles with no known central component, 21 classical doubles with central components, and 2 asymmetrical doubles. I have been unable to find core flux values for 4 of the doubles for which cores have been detected with the VLA.

Table 1 lists the observational properties of the sources. Col. 1 is the name, col 2 the redshift. Redshifts of exactly 1 are guesses. Col 3 gives the S_{178} flux from ref (1). The next 4 columns are fluxes at 5 GHz, the first from various references listed in the first column of references at the right hand end of the table, the second from ref (2), the third is the central component flux (from refs in 2nd col of

reference nos.) and the fourth the difference between the third and first columns of 5 GHz fluxes, ie the flux of the extended structure. The next 2 columns give spectral indices from refs (1) & (2), and finally angular diameter in arcsec is listed. The 3rd column of references gives the source of the maps of each object.

Of this data, the Laing & Peacock fluxes and spectral indices are for comparison only and have not been used. P_{178} is calculated using the first set of spectral indices, but P_e and P_c are calculated using spectral indices of 0.8 and 0 respectively. Table 2 lists the calculated values of the projected physical diameter d, the flux ratio R_{obs}, and the P_{178} and P_{5000} luminosities for various values of H_0 and Ω. Table 3 lists the 5 GHz luminosities calculated using the various alternative combinations of fluxes and spectral index; these numbers are ignored henceforth. Fig. 1 shows the distribution of the sources in redshift space.

3. The Luminosity distribution

If the model were correct one might naively expect that compact quasars should be brighter than classical doubles, since they are beamed up until the core dominates the lobes. However the luminosity distribution of fig. 10 shows that there is little difference in the luminosities of double and compact quasars. This implies that in our model the Lorentz factor must be high enough to restrict the beaming to a very small solid angle, so that we see none of the doubles as bright as 3C objects end on, and all of our compact

objects have lobe luminosities which are lower than those in our sample.

There is no correlation observed between R_{obs} and total 178 MHz luminosity, (the rank correlation coefficient, Spearman's ρ, is -0.22 which is not significant at the 5% level) but as might be expected, R_{obs} and P_c are correlated ($\rho = 0.60$ for 19 points which is significant at the 1% level; Pearson's $r = 0.70$, [see Fig. 3]

4. The size distribution for double sources.

The angular diameter distribution is shown in fig. 2. The corresponding distributions of projected size d and of $\log d$ are shown in figs. 5 and 11. If the hypothesis is correct we expect the highest R_{obs} values to go with the smallest projected sizes; Fig. 4 shows diameter versus $\log R_{obs}$ and the rank correlation coefficient is -0.45 ($\Omega_0 = 0$) or -0.48 ($\Omega_0 = 1$) which is significant at the 5% level but not the 1% level. In particular there are a number of objects with high R_{obs} and high d, and also low R_{obs} and low d. Hence we require a fair scatter in deprojected, true physical size D.

Because of the $\cos\theta$ distribution, most of the objects are seen with large θ, so $d \simeq D$. We may ask the question: If there are n quasars in a given d bin, d_0, how many objects in bins of lower d are of the same physical size $D \sim d_0$ but foreshortened by projection?

For the $P(\log d)$ distribution this is simple as the answer is d-independent. The bin size is 0.2 in $\log d$; If we assume all the objects in the n^{th} bin are of deprojected size D_0 then the number of objects in the bins of lower d may be found from the table below:

Bin	θ range	% of total	% of bin n
n	39° - 90	77.6	100
n-1	23 - 39	14.2	18
n-2	14 - 23	5.0	6.4
n-3	9 - 14	2.0	2.5
n-4	5 - 9	0.8	1.0

The P(d) distribution requires a different value for each bin.
The distribution for $H_0 = 50$ shows a sharp peak at d = 100 to 150.
Assuming all 8 of these objects (for $\Omega = 1$) to be of intrinsic size 150 kpc gives a prediction of 2 in the 50 - 100 kpc bin and 0.6 in the 0 - 50 kpc bin. There are indeed 2 sources in the 50 - 100 kpc bin which have the brightest : flux ratios of all except the asymmetrical doubles, (3C 207 & 212). The other sources in this bin are 3C 9, 208, and 268.4; and also 3C 181 (no central component). For $\Omega = 0$ there are 4 sources in the relevant bin, 3C 207, 3C 196, 3C 245, and 3C 181.

5. Modelling the distribution of R_{obs}

Fig 12 & 13 show the form of the function $R(\gamma, \theta)$: given R and γ we may find θ by successive approximation; given γ and assuming a uniform distribution in $\cos\theta$ we may predict the probability distribution of R, and hence of R_{obs} given a choice of λ.

$$P(\log R_0 < \log R < \log R_1) = \int_{R_0}^{R_1} \frac{d\cos\theta}{d\log R}\, d\log R$$

$$= \cos\theta_1 - \cos\theta_0$$

$$\log R_{obs} = \log R - \log \gamma^3\lambda$$

[I find θ by using $y = (1-\cos\theta)$ & $y_{new} = (2R\gamma^3 + (y-2)_{old}^{-3})^{-1/3}$ which converges rapidly.]

The distribution $P(\log R_{obs})$ has been plotted in fig. 14 for different values of γ but with λ chosen to keep the peak (& maximum value of R_{obs}) at $R_{obs} = \frac{1}{\gamma^3\lambda} = 10^{-1.5}$ to agree with that observed in ($\log R_{obs}$) plotted in fig 15. Obviously the low-R tail cannot be modelled by the same value of γ and λ as the peak, but the sharpness of the peak (width ~ 0.4 in $\log_{10}$) includes a range in $\gamma^3\lambda$ for constant γ of a factor of about 2.5, or in γ for constant λ of 1.4 (since the position of the peak is a function of $\gamma^3\lambda$). Increasing γ keeping λ const, or increasing λ keeping γ constant, will move the peak toward lower values of R_{obs}. At high γ the distribution tends rapidly to a limiting one as $\beta = \frac{v}{c} \to 1$, $\gamma \to \infty$ and $\gamma^3\lambda = \text{const}$. The limit has essentially been reached by $\gamma = 10$. Of course it may be that the distribution of R is due to random scatter in λ and has nothing to do with any beaming. In fact the $\log R$ distribution is indistinguishable from a normal distribution at the 20% level with the Lilliefors normality test.

γ & λ values for $R_{obs,peak} = \frac{1}{31.6} = 10^{-1.5}$

γ	λ
1.3	14.4
1.5	9.4
2	4.0
5	0.25
10	0.032

For given γ, these values of λ are the minimum ones to explain the ~~data~~ majority of the data. If smaller values ~~For γ~~ are chosen, the R_{obs} values cannot be reproduced. If much larger λ values are chosen, the deprojected distribution is squashed into a small range of high $\cos\theta$, and the objects with large $\cos\theta$ will appear largest in 'actual' size.

If we fix γ & λ, then taking a high value of γ should push the sources into a small range of low $\cos\theta$, and the objects near the line of sight will appear smaller in deprojected size.

We may test the hypothesis that the distribution obtained is uniform in $\cos\theta$ by using the Kolmogorov–Smirnov test. If $F_n(\cos\theta)$ is the observed cumulative distribution and $F(\cos\theta) = \cos\theta$ is the predicted one, the statistic

$$K_n = \sqrt{n} \sup_{0 \le \cos\theta \le 1} |F_n(\cos\theta) - \cos\theta|$$

is distributed such that

$$P(K_n \ge x) \approx 2e^{-2x^2} \quad \text{for } x \gtrsim 1,$$
$$\approx \sum_{j=1}^{\infty} 2(-1)^{j-1} e^{-2j^2x^2} \quad \text{for all } x.$$

(small n correction factor: $K_n \to \frac{K_n}{1 - 0.53n^{-0.9}}$)

Now we must consider the objects for which we have no core values. First we may suppose that they have cores typical

of those we do have data for, or that they have lower R_{obs} values due to higher γ or λ; in this case we expect our 15 R_{obs} values, with $\log R_{obs} \geq -1.5$ to give us a uniform distribution in $\cos\theta$ with $\gamma^3\lambda \sim \frac{1}{32}$. Secondly, we may suppose that the unknown cores have lower R_{obs} values but come from the same distribution, ie. same $\gamma \& \lambda$; ~~then if we assume these k objects~~ Suppose these objects lie all in the bin $-2 \leq \log R_{obs} \leq -1.5$; then $\gamma^3\lambda \sim 10^{-2}$ and we assume the k objects in this bin are indeed uniformly distributed in $\cos\theta$, and can test the difference between the distribution of the (k+n) objects and a uniform distribution using $K_n = \sqrt{n} \sup_{\cos\theta_1 \leq \cos\theta \leq 1} |F_n(\cos\theta) - \cos\theta|$ where $F_n(\cos\theta)$ for the 1st object we have data for is $\frac{k+1}{k+n}$, not $\frac{1}{n}$. We are thus asking the question: are there too many objects in the second and third bins to be compatible with a population peaking in the first bin.

From the calculations in Table 4, based on the deprojections in Fig. 16 (a)-(g), we find (n = 15)

			Small n correction	K_n
$\gamma = 2$	$\lambda = 4$	$K_n = 0.58$	X 1.04	0.60
$\gamma = 5$	$\lambda = 0.25$	$K_n = 0.93$		0.97
$\gamma = 10$	$\lambda = 0.032$	$K_n = 0.97$		1.01
$\gamma = 2$	$\lambda = 12.4$	$K_n = 0.89$		0.93 with 6 objects assumed in lower bin
$\gamma = 5$	$\lambda = 0.78$	$K_n = 0.66$		0.69 "

None of these hypotheses can be rejected at any sensible level. On the other hand, a model with single very small values of γ can be rejected as the range of beaming would be too small; for the distribution to be as broad in the tail and as narrow at the peak as it is, γ must be typically at least 1.5.

$\gamma = 1.3$	$\lambda = 14.4$	7 points	$K_n = 0.62$
$\gamma = 1.5$	$\lambda = 9.4$	14 points	$K_n = 0.60$

(Fig 16 h, j)

6. The spread in γ

Monte carlo simulations were performed for given values of λ, choosing random values of $\cos\theta$ to give $P(\gamma) = \left(\frac{d\cos\theta}{d\gamma}\right)_\lambda$ for the R_{obs} values in the data set.

At large γ for a single R value the curve has the form $(2R)^{-1/3} \cdot \frac{1}{\gamma^2}$

(The full form is:

$$P(\gamma) = \frac{2R\gamma^2}{f(\gamma,\theta)\left(1-\frac{1}{\gamma^2}\right)^{1/2}} - \frac{\cos\theta(\gamma,R)}{\gamma^3-\gamma}$$

$$f(\gamma,\theta) = \frac{1}{(1-\beta\cos\theta)^4} - \frac{1}{(1+\beta\cos\theta)^4}$$)

Fig 17 shows the generated distributions of γ; the $\gamma < 1$ bin shows the proportion of trials for which the chosen $\cos\theta$ yielded no real γ value.

λ	Percentage rejection
0.5	0
1	4
2	4.4
3	11.6
4	15%
9.4	26%
14.4	34%

For smaller λ values the γ cutoff is given by the maximum R_{obs} value of 1.703 and is $\frac{1}{(1.7\lambda)^{1/3}}$ The spread in γ is typically 1.5 to 6

7. 'Allowed' values of γ, λ.

A rough estimate of the allowed region in the γ, λ plane may be made by calculating K_n for many different γ, λ values. The program I have used to do this does not reject R_{obs} values for which there is no solution but sets $\cos\theta$ to 0 or 1 as appropriate; it has been used to calculate K_n for the 15 data points with $\log R_{obs} \geq 1.5$, and the form of the low γ end of the K_n contour plot (fig. 18) is due to the range of beaming factors becoming too small to explain all the values of R_{obs}. The plot shows the line $\log \gamma^3\lambda = 1.5$ and contours of the 10, 5 and 1 percent significance levels of the test in $\log\gamma$, $\log\lambda$ space. The 1% level allows values of $\gamma^3\lambda$ between 14 and 100. (5%: 16 to 71; 10%: 17 to 59) (Program: J. GALAXY)

8. The sample again

If the compact sources are end-on doubles, then if γ is only 2, and $\lambda = 4$, the contribution to the flux from the lobes is at least 13% of total 5 GHz flux (and more at lower frequencies) since the maximum beaming factor is 26.

γ	λ	% of total flux in lobes $= \frac{\lambda}{R(\theta)+\lambda}$		
		$\cos\theta = 1$	0.95	0.9
5	0.25	0.05	2	9
4	0.5	0.2	3.2	12
3	1.17	1.2	6.7	18
2	4	13	26	41

Limits on γ from the doubles

If γ is very large, the doubles with cores we observe must be highly debeamed, but only a very small proportion will be highly beamed. The table below gives the required $\cos\theta$ for R_{obs} to be 1, 10, and 20.

γ	λ	$\cos\theta$, $R_{obs}=1$	10	20
20	0.004	0.995	0.998	0.999
10	0.032	0.980	0.993	0.996
5	0.25	0.919	0.973	0.983
4	0.5	0.870	0.957	0.973
3	1.17	0.765	0.923	0.952
2	4	0.400	0.817	0.887.

The end

1 Laing R.A. Riley J.M. Longair M.S. (1982) MNRAS, in press

2 Laing R.A. Peacock J.A. (1980) MNRAS, 190, 203

3 Pooley G.G. Henbest S.N. (1974) MNRAS, 169, 477

4 Jenkins, CJ Pooley G G Riley J M (1977) MemRAS 84, 61

5 Laing R.A Unpublished

6 Stocke J., Christiansen W Burns J (1982) IAU Sym 97, p.39

7 Riley J M Pooley G G (1975) MemRAS 80, 105

8 Laing R A (1981) MNRAS 194, 301

9 Laing R A (1982) IAU Sym 97, p 161

10 Wardle JFC Potash R (1982) IAU Sym 97, p 129

11 Kronberg PP Clarke J N van den Bergh S (1980) AJ 85, 973

12 Swarup, G Sinha R & Saikia D (1982) TIFR preprint, RoE no 82464, MNRAS in prep

13 Browne IWA Orr MJL Davis RJ Foley A Muxlow TWB Thomasson P (1982) MN 198, 673

14 Schilizzi R, Kapahi VK, Neff SG (1982) TIFR preprint, [JAstroph & Astron in press] RoE no 82465

15 Preuss E · Alef W Pauliny Tóth I Kellerman KI (1982) IAU 97, p 289

QSO	Z	S 178 (1)	S 5000 REF 1	S 5000 (2)	S CORE 5000 REF 2	S E 5000 R1-2	SI LF (1)	SI HF (2)	ANG DIA "	REFS 1	REFS 2	MAP	TYPE CODE
CLASSICAL DOUBLES WITH CENTRAL COMPONENTS													
3C 9	2.012	17.8	0.48	0.55	0.0000	0.48	1.12	1.06	10.0	3	0	12	1
3C 47	0.425	26.4	1.06	1.09	0.0800	0.98	0.98	0.95	69.0	3	3	3	1
3C175	0.768	17.6	0.67	0.65	0.0400	0.63	0.98	1.03	48.0	4	4	4	1
3C190	1.197	15.0	0.83	0.81	0.0000	0.83	0.93	0.88	2.4	4	0	8	1
3C191	1.956	13.0	0.59	0.46	0.0000	0.59	0.98	1.02	3.4	4	0	8	1
3C196	0.871	68.2	4.50	4.33	0.0000	4.50	0.79	0.90	5.0	3	0	9	1
3C204	1.112	10.5	0.40	0.34	0.0400	0.36	1.08	1.08	31.0	3	3	3	1
3C205	1.534	12.6	0.72	0.67	0.0300	0.69	0.88	0.98	16.0	3	3	3	1
3C207	0.684	13.6	1.24	1.43	0.5100	0.73	0.90	0.55	8.4	3	3	3	1
3C208	1.110	16.8	0.58	0.54	0.0540	0.53	0.96	1.19	11.0	4	4	5	1
3C212	1.049	15.1	0.98	0.88	0.3100	0.67	0.92	0.86	9.0	4	4	4	1
3C215	0.411	11.4	0.33	0.41	0.0200	0.31	1.06	1.04	28.5	3	3	3	1
3C249.1	0.311	10.7	0.69	0.78	0.1100	0.58	0.81	0.82	23.0	3	3	3	1
3C254	0.734	19.9	0.83	0.78	0.0197	0.81	0.96	1.04	13.2	3	5	5	1
3C263	0.656	15.2	1.03	1.03	0.1300	0.90	0.82	0.85	44.0	3	3	3	1
3C268.4	1.400	10.3	0.73	0.60	0.0500	0.68	0.80	0.96	10.2	3	3	14	1
3C270.1	1.519	13.6	1.54	0.86	0.1920	1.35	0.75	0.93	12.0	6	6	6	1
3C275.1	0.557	18.3	1.33	0.90	0.1350	1.19	0.96	0.92	14.0	6	6	6	1
3C325	1.000	15.6	1.10	0.82	0.0054	1.05	0.70	1.02	16.0	4	5	5	1
3C334	0.555	10.9	0.72	0.57	0.1700	0.55	0.86	0.90	48.0	4	4	10	1
3C351	0.371	13.7	1.25	1.20	0.0150	1.23	0.73	0.78	58.0	7	7	11	1
ASYMMETRIC DOUBLES													
3C245	1.029	14.4	1.60	1.38	1.2000	0.40	0.78	0.68	4.6	4	4	8	4
3C455	0.543	12.8	0.84	0.92	0.3000	0.54	0.71	0.94	3.2	4	4	4	4
DOUBLES WITHOUT CENTRAL COMPONENT													
3C 14	1.000	10.4	0.64	0.61	0.0000	0.64	0.81	0.93	24.0	4	0	4	2
3C 68.1	1.238	12.8	0.80	0.82	0.0000	0.80	0.80	0.88	46.0	4	0	4	2
3C181	1.382	14.5	0.80	0.66	0.0000	0.80	1.00	0.91	5.9	3	0	3	2
3C336	0.927	11.5	0.76	0.69	0.0000	0.76	0.73	0.95	21.7	3	0	3	2
4C 16.49	1.000	10.5	0.40	0.00	0.0000	0.40	1.00	0.00	16.0	1	0	1	2
3C432	1.805	11.0	1.76	0.31	0.0000	1.76	0.98	1.07	13.0	4	0	4	2
COMPACT QUASARS													
3C 43	1.457	11.6	0.00	1.08	1.0800	0.00	0.75	0.74	1.0	4	0	0	3
3C 48	0.367	55.0	0.00	5.33	5.3300	0.00	0.59	0.83	0.0	0	0	0	3
3C138	0.759	22.2	0.00	4.13	4.1300	0.00	0.46	0.58	0.0	0	0	0	3
3C147	0.545	60.5	0.00	8.12	8.1200	0.00	0.46	0.77	0.3	0	0	15	3
3C186	1.063	14.1	0.00	0.38	0.3800	0.00	1.15	1.13	2.7	7	0	14	3
3C216	0.668	20.2	0.00	1.80	1.8000	0.00	0.84	0.67	0.8	4	0	14	3
3C287	1.055	16.3	0.00	3.24	3.2400	0.00	0.42	0.58	0.0	0	0	0	3
3C286	0.849	25.0	0.00	7.43	7.4300	0.00	0.24	0.51	0.1	0	0	0	3
3C309.1	0.904	22.7	0.00	3.73	3.7300	0.00	0.53	0.60	2.0	0	0	8	3
3C343	0.988	12.4	0.00	1.48	1.4800	0.00	0.37	0.91	0.0	0	0	0	3
3C345	0.594	10.8	0.00	5.61	5.6100	0.00	0.27	0.17	6.0	0	0	13	3
3C380	0.691	59.4	0.00	7.45	7.4500	0.00	0.71	0.58	0.0	4	0	0	3
3C454	1.757	11.6	0.00	0.78	0.7800	0.00	0.90	0.79	0.5	4	0	0	3
3C454.3	0.860	13.0	0.00	19.57	19.570	0.00	0.04	-0.14	6.0	0	0	13	3

'JCM.DATA.CAMOUT'

Notes

Z redshift

S Flux in Jy

S_{178} from (1)

S_{5000} from both (2) and the reference in the column 'REFS 1'

S_{CORE}, S_{GHz} from the reference in the column 'REFS 2'

SE is defined as $S_{5000(REFS1)} - S_{CORE}$

SI : spectral indices, low & high frequency, from (1) & (2) respectively

ANG DIA mostly from the same sources as the maps given in the third column of references.

Table 1

HO=50 OMEGA=0

QSO	DIA	R	P178	P EXT	P CORE
CLASSICAL DOUBLES					
3C 9.0	129.	0.000	0.113E+30	0.215E+28	0.000E+01
3C 47.0	509.	0.061	0.238E+28	0.830E+26	0.510E+25
3C175.0	474.	0.040	0.673E+28	0.217E+27	0.875E+25
3C190.0	28.	0.000	0.178E+29	0.889E+27	0.000E+01
3C191.0	44.	0.000	0.652E+29	0.243E+28	0.000E+01
3C196.0	52.	0.000	0.320E+29	0.212E+28	0.000E+01
3C204.0	350.	0.061	0.114E+29	0.318E+27	0.194E+26
3C205.0	196.	0.021	0.283E+29	0.144E+28	0.298E+26
3C207.0	79.	0.460	0.372E+28	0.190E+27	0.874E+26
3C208.0	124.	0.056	0.166E+29	0.466E+27	0.261E+26
3C212.0	100.	0.261	0.125E+29	0.508E+27	0.132E+27
3C215.0	206.	0.049	0.978E+27	0.243E+26	0.119E+25
3C249.1	140.	0.153	0.449E+27	0.243E+26	0.371E+25
3C254.0	128.	0.016	0.671E+28	0.250E+27	0.392E+25
3C263.0	406.	0.096	0.361E+28	0.211E+27	0.204E+26
3C268.4	123.	0.036	0.168E+29	0.111E+28	0.404E+26
3C270.1	147.	0.068	0.264E+29	0.274E+28	0.186E+27
3C275.1	120.	0.080	0.312E+28	0.189E+27	0.151E+26
3C325.0	174.	0.003	0.976E+28	0.704E+27	0.208E+25
3C334.0	409.	0.217	0.176E+28	0.866E+26	0.188E+26
3C351.0	395.	0.009	0.833E+27	0.765E+26	0.725E+24
3C245.0	51.	1.703	0.102E+29	0.289E+27	0.492E+27
3C455.0	27.	0.393	0.184E+28	0.808E+26	0.317E+26
DOUBLES WITHOUT CENTRAL COMPONENTS					
3C 14.0	262.	0.000	0.702E+28	0.429E+27	0.000E+01
3C 68.1	535.	0.000	0.150E+29	0.936E+27	0.000E+01
3C181.0	71.	0.000	0.271E+29	0.126E+28	0.000E+01
3C336.0	230.	0.000	0.607E+28	0.420E+27	0.000E+01
4C16.49	174.	0.000	0.809E+28	0.268E+27	0.000E+01
3C432.0	165.	0.000	0.435E+29	0.578E+28	0.000E+01
COMPACT QUASARS					
3C 43.0	12.	0.000	0.201E+29	0.000E+01	0.954E+27
3C 48.0	0.	0.000	0.312E+28	0.000E+01	0.252E+27
3C138.0	0.	0.000	0.614E+28	0.000E+01	0.881E+27
3C147.0	3.	0.000	0.788E+28	0.000E+01	0.865E+27
3C186.0	30.	0.000	0.143E+29	0.000E+01	0.167E+27
3C216.0	7.	0.000	0.506E+28	0.000E+01	0.293E+27
3C287.0	0.	0.000	0.954E+28	0.000E+01	0.140E+28
3C286.0	1.	0.000	0.785E+28	0.000E+01	0.201E+28
3C309.1	21.	0.000	0.989E+28	0.000E+01	0.116E+28
3C343.0	0.	0.000	0.600E+28	0.000E+01	0.555E+27
3C345.0	53.	0.000	0.156E+28	0.000E+01	0.715E+27
3C380.0	0.	0.000	0.151E+29	0.000E+01	0.130E+28
3C454.0	6.	0.000	0.391E+29	0.000E+01	0.106E+28
3C454.3	62.	0.000	0.371E+28	0.000E+01	0.545E+28

HO=50 OMEGA=1

QSO	DIA	R	P178	P EXT	P CORE
CLASSICAL DOUBLES					
3C 9.0	82.	0.000	0.453E+29	0.859E+27	0.000E+01
3C 47.0	457.	0.061	0.192E+28	0.669E+26	0.411E+25
3C175.0	391.	0.040	0.458E+28	0.148E+27	0.595E+25
3C190.0	21.	0.000	0.993E+28	0.496E+27	0.000E+01
3C191.0	28.	0.000	0.266E+29	0.995E+27	0.000E+01
3C196.0	42.	0.000	0.207E+29	0.138E+28	0.000E+01
3C204.0	266.	0.061	0.662E+28	0.184E+27	0.113E+26
3C205.0	136.	0.021	0.137E+29	0.696E+27	0.144E+26
3C207.0	67.	0.460	0.264E+28	0.134E+27	0.619E+26
3C208.0	94.	0.056	0.965E+28	0.270E+27	0.151E+26
3C212.0	77.	0.261	0.745E+28	0.303E+27	0.790E+26
3C215.0	186.	0.049	0.793E+27	0.197E+26	0.966E+24
3C249.1	129.	0.153	0.384E+27	0.207E+26	0.317E+25
3C254.0	106.	0.016	0.464E+28	0.173E+27	0.271E+25
3C263.0	344.	0.096	0.259E+28	0.152E+27	0.146E+26
3C268.4	88.	0.036	0.857E+28	0.566E+27	0.206E+26
3C270.1	102.	0.068	0.128E+29	0.133E+28	0.906E+26
3C275.1	104.	0.080	0.235E+28	0.143E+27	0.114E+26
3C325.0	136.	0.003	0.595E+28	0.429E+27	0.127E+25
3C334.0	355.	0.217	0.133E+28	0.654E+26	0.142E+26
3C351.0	359.	0.009	0.690E+27	0.633E+26	0.600E+24
3C245.0	39.	1.703	0.617E+28	0.174E+27	0.296E+27
3C455.0	24.	0.393	0.140E+28	0.614E+26	0.241E+26
DOUBLES WITHOUT CENTRAL COMPONENTS					
3C 14.0	204.	0.000	0.428E+28	0.262E+27	0.000E+01
3C 68.1	396.	0.000	0.821E+28	0.513E+27	0.000E+01
3C181.0	51.	0.000	0.140E+29	0.648E+27	0.000E+01
3C336.0	183.	0.000	0.383E+28	0.265E+27	0.000E+01
4C16.49	136.	0.000	0.493E+28	0.164E+27	0.000E+01
3C432.0	109.	0.000	0.188E+29	0.250E+28	0.000E+01
COMPACT QUASARS					
3C 43.0	9.	0.000	0.100E+29	0.000E+01	0.476E+27
3C 48.0	0.	0.000	0.259E+28	0.000E+01	0.209E+27
3C138.0	0.	0.000	0.420E+28	0.000E+01	0.602E+27
3C147.0	2.	0.000	0.597E+28	0.000E+01	0.656E+27
3C186.0	23.	0.000	0.845E+28	0.000E+01	0.991E+26
3C216.0	6.	0.000	0.361E+28	0.000E+01	0.209E+27
3C287.0	0.	0.000	0.568E+28	0.000E+01	0.834E+27
3C286.0	1.	0.000	0.514E+28	0.000E+01	0.132E+28
3C309.1	17.	0.000	0.631E+28	0.000E+01	0.737E+27
3C343.0	0.	0.000	0.368E+28	0.000E+01	0.341E+27
3C345.0	46.	0.000	0.116E+28	0.000E+01	0.529E+27
3C380.0	0.	0.000	0.107E+29	0.000E+01	0.920E+27
3C454.0	4.	0.000	0.173E+29	0.000E+01	0.466E+27
3C454.3	50.	0.000	0.242E+28	0.000E+01	0.355E+28

Table 2(c)

HO=100 OMEGA=0

QSO	DIA	R	P178	P EXT	P CORE
CLASSICAL DOUBLES					
3C 9.0	65.	0.000	0.283E+29	0.537E+27	0.000E+01
3C 47.0	254.	0.061	0.596E+27	0.207E+26	0.128E+25
3C175.0	237.	0.040	0.168E+28	0.544E+26	0.219E+25
3C190.0	14.	0.000	0.445E+28	0.222E+27	0.000E+01
3C191.0	22.	0.000	0.163E+29	0.609E+27	0.000E+01
3C196.0	26.	0.000	0.800E+28	0.531E+27	0.000E+01
3C204.0	175.	0.061	0.286E+28	0.794E+26	0.485E+25
3C205.0	98.	0.021	0.709E+28	0.360E+27	0.744E+25
3C207.0	40.	0.460	0.931E+27	0.474E+26	0.218E+26
3C208.0	62.	0.056	0.416E+28	0.116E+27	0.653E+25
3C212.0	50.	0.261	0.312E+28	0.127E+27	0.331E+26
3C215.0	103.	0.049	0.244E+27	0.608E+25	0.298E+24
3C249.1	70.	0.153	0.112E+27	0.607E+25	0.927E+24
3C254.0	64.	0.016	0.168E+28	0.625E+26	0.979E+24
3C263.0	203.	0.096	0.902E+27	0.528E+26	0.510E+25
3C268.4	61.	0.036	0.419E+28	0.277E+27	0.101E+26
3C270.1	73.	0.068	0.660E+28	0.686E+27	0.466E+26
3C275.1	60.	0.080	0.780E+27	0.473E+26	0.376E+25
3C325.0	87.	0.003	0.244E+28	0.176E+27	0.520E+24
3C334.0	205.	0.217	0.441E+27	0.217E+26	0.470E+25
3C351.0	197.	0.009	0.208E+27	0.191E+26	0.181E+24
3C245.0	25.	1.703	0.256E+28	0.722E+26	0.123E+27
3C455.0	13.	0.393	0.460E+27	0.202E+26	0.793E+25
DOUBLES WITHOUT CENTRAL COMPONENTS					
3C 14.0	131.	0.000	0.176E+28	0.107E+27	0.000E+01
3C 68.1	268.	0.000	0.375E+28	0.234E+27	0.000E+01
3C181.0	35.	0.000	0.678E+28	0.314E+27	0.000E+01
3C336.0	115.	0.000	0.152E+28	0.105E+27	0.000E+01
4C16.49	87.	0.000	0.202E+28	0.671E+26	0.000E+01
3C432.0	82.	0.000	0.109E+29	0.145E+28	0.000E+01
COMPACT QUASARS					
3C 43.0	6.	0.000	0.503E+28	0.000E+01	0.239E+27
3C 48.0	0.	0.000	0.781E+27	0.000E+01	0.630E+26
3C138.0	0.	0.000	0.154E+28	0.000E+01	0.220E+27
3C147.0	1.	0.000	0.197E+28	0.000E+01	0.216E+27
3C186.0	15.	0.000	0.357E+28	0.000E+01	0.418E+26
3C216.0	4.	0.000	0.126E+28	0.000E+01	0.733E+26
3C287.0	0.	0.000	0.239E+28	0.000E+01	0.350E+27
3C286.0	1.	0.000	0.196E+28	0.000E+01	0.503E+27
3C309.1	11.	0.000	0.247E+28	0.000E+01	0.289E+27
3C343.0	0.	0.000	0.150E+28	0.000E+01	0.139E+27
3C345.0	26.	0.000	0.390E+27	0.000E+01	0.179E+27
3C380.0	0.	0.000	0.377E+28	0.000E+01	0.326E+27
3C454.0	3.	0.000	0.977E+28	0.000E+01	0.264E+27
3C454.3	31.	0.000	0.927E+27	0.000E+01	0.136E+28

HO=100 OMEGA=1

QSO	DIA	R	P178	P EXT	P CORE
CLASSICAL DOUBLES					
3C 9.0	41.	0.000	0.113E+29	0.215E+27	0.000E+01
3C 47.0	228.	0.061	0.480E+27	0.167E+26	0.103E+25
3C175.0	196.	0.040	0.114E+28	0.370E+26	0.149E+25
3C190.0	10.	0.000	0.248E+28	0.124E+27	0.000E+01
3C191.0	14.	0.000	0.666E+28	0.249E+27	0.000E+01
3C196.0	21.	0.000	0.518E+28	0.344E+27	0.000E+01
3C204.0	133.	0.061	0.166E+28	0.460E+26	0.281E+25
3C205.0	68.	0.021	0.342E+28	0.174E+27	0.360E+25
3C207.0	33.	0.460	0.659E+27	0.336E+26	0.155E+26
3C208.0	47.	0.056	0.241E+28	0.675E+26	0.379E+25
3C212.0	38.	0.261	0.186E+28	0.758E+26	0.198E+26
3C215.0	93.	0.049	0.198E+27	0.493E+25	0.242E+24
3C249.1	65.	0.153	0.959E+26	0.518E+25	0.792E+24
3C254.0	53.	0.016	0.116E+28	0.432E+26	0.677E+24
3C263.0	172.	0.096	0.647E+27	0.380E+26	0.366E+25
3C268.4	44.	0.036	0.214E+28	0.141E+27	0.516E+25
3C270.1	51.	0.068	0.321E+28	0.334E+27	0.227E+26
3C275.1	52.	0.080	0.588E+27	0.356E+26	0.284E+25
3C325.0	68.	0.003	0.149E+28	0.107E+27	0.317E+24
3C334.0	178.	0.217	0.333E+27	0.164E+26	0.355E+25
3C351.0	179.	0.009	0.172E+27	0.158E+26	0.150E+24
3C245.0	20.	1.703	0.154E+28	0.434E+26	0.740E+26
3C455.0	12.	0.393	0.350E+27	0.153E+26	0.602E+25
DOUBLES WITHOUT CENTRAL COMPONENTS					
3C 14.0	102.	0.000	0.107E+28	0.654E+26	0.000E+01
3C 68.1	198.	0.000	0.205E+28	0.128E+27	0.000E+01
3C181.0	25.	0.000	0.349E+28	0.162E+27	0.000E+01
3C336.0	92.	0.000	0.957E+27	0.662E+26	0.000E+01
4C16.49	68.	0.000	0.123E+28	0.409E+26	0.000E+01
3C432.0	54.	0.000	0.471E+28	0.626E+27	0.000E+01
COMPACT QUASARS					
3C 43.0	4.	0.000	0.251E+28	0.000E+01	0.119E+27
3C 48.0	0.	0.000	0.648E+27	0.000E+01	0.522E+26
3C138.0	0.	0.000	0.105E+28	0.000E+01	0.151E+27
3C147.0	1.	0.000	0.149E+28	0.000E+01	0.164E+27
3C186.0	12.	0.000	0.211E+28	0.000E+01	0.248E+26
3C216.0	3.	0.000	0.903E+27	0.000E+01	0.524E+26
3C287.0	0.	0.000	0.142E+28	0.000E+01	0.208E+27
3C286.0	0.	0.000	0.128E+28	0.000E+01	0.329E+27
3C309.1	8.	0.000	0.158E+28	0.000E+01	0.184E+27
3C343.0	0.	0.000	0.920E+27	0.000E+01	0.852E+26
3C345.0	23.	0.000	0.289E+27	0.000E+01	0.132E+27
3C380.0	0.	0.000	0.266E+28	0.000E+01	0.230E+27
3C454.0	2.	0.000	0.431E+28	0.000E+01	0.116E+27
3C454.3	25.	0.000	0.604E+27	0.000E+01	0.887E+27

Table 3 (a)

Luminosities calculated using alternative fluxes and spectral indices

H0=50 OMEGA=0

3C R P5000 SI	; HF	REF1,HF	REF1,.8	LP,HF	LP, .8	EXT,HF
CLASSICAL DOUBLES						
9.0	0.000	0.286E+28	0.215E+28	0.328E+28	0.246E+28	0.286E+28
47.0	0.058	0.947E+26	0.898E+26	0.973E+26	0.923E+26	0.875E+26
175.0	0.035	0.264E+27	0.231E+27	0.256E+27	0.224E+27	0.248E+27
190.0	0.000	0.946E+27	0.889E+27	0.924E+27	0.867E+27	0.946E+27
191.0	0.000	0.309E+28	0.243E+28	0.241E+28	0.190E+28	0.309E+28
196.0	0.000	0.226E+28	0.212E+28	0.218E+28	0.204E+28	0.226E+28
204.0	0.050	0.435E+27	0.353E+27	0.370E+27	0.300E+27	0.392E+27
205.0	0.017	0.178E+28	0.150E+28	0.165E+28	0.140E+28	0.170E+28
207.0	0.525	0.283E+27	0.322E+27	0.326E+27	0.372E+27	0.167E+27
208.0	0.042	0.682E+27	0.509E+27	0.635E+27	0.474E+27	0.623E+27
212.0	0.250	0.776E+27	0.743E+27	0.697E+27	0.667E+27	0.531E+27
215.0	0.045	0.281E+26	0.259E+26	0.349E+26	0.322E+26	0.264E+26
249.1	0.152	0.291E+26	0.289E+26	0.328E+26	0.327E+26	0.244E+26
254.0	0.014	0.292E+27	0.256E+27	0.275E+27	0.241E+27	0.285E+27
263.0	0.094	0.248E+27	0.242E+27	0.248E+27	0.242E+27	0.217E+27
268.4	0.032	0.137E+28	0.119E+28	0.112E+28	0.977E+27	0.127E+28
270.1	0.060	0.353E+28	0.313E+28	0.197E+28	0.175E+28	0.309E+28
275.1	0.075	0.223E+27	0.211E+27	0.151E+27	0.143E+27	0.199E+27
325.0	0.003	0.859E+27	0.738E+27	0.640E+27	0.550E+27	0.820E+27
334.0	0.208	0.119E+27	0.113E+27	0.939E+26	0.898E+26	0.906E+26
351.0	0.010	0.772E+26	0.777E+26	0.741E+26	0.746E+26	0.760E+26
245.0	1.854	0.106E+28	0.115E+28	0.915E+27	0.996E+27	0.265E+27
455.0	0.370	0.134E+27	0.126E+27	0.146E+27	0.138E+27	0.859E+26
DOUBLES WITHOUT CENTRAL COMPONENTS						
14.0	0.000	0.470E+27	0.429E+27	0.448E+27	0.409E+27	0.470E+27
68.1	0.000	0.999E+27	0.936E+27	0.102E+28	0.960E+27	0.999E+27
181.0	0.000	0.138E+28	0.126E+28	0.114E+28	0.104E+28	0.138E+28
336.0	0.000	0.463E+27	0.420E+27	0.421E+27	0.381E+27	0.463E+27
16.5	0.000	0.154E+27	0.268E+27	0.000E+01	0.000E+01	0.154E+27
432.0	0.000	0.764E+28	0.578E+28	0.135E+28	0.102E+28	0.764E+28
COMPACT QUASARS						
43.0	0.000	0.000E+01	0.000E+01	0.186E+28	0.196E+28	0.000E+01
48.0	0.000	0.000E+01	0.000E+01	0.326E+27	0.323E+27	0.000E+01
138.0	0.000	0.000E+01	0.000E+01	0.122E+28	0.138E+28	0.000E+01
147.0	0.000	0.000E+01	0.000E+01	0.121E+28	0.123E+28	0.000E+01
186.0	0.000	0.000E+01	0.000E+01	0.379E+27	0.298E+27	0.000E+01
216.0	0.000	0.000E+01	0.000E+01	0.413E+27	0.442E+27	0.000E+01
287.0	0.000	0.000E+01	0.000E+01	0.213E+28	0.249E+28	0.000E+01
286.0	0.000	0.000E+01	0.000E+01	0.275E+28	0.329E+28	0.000E+01
309.1	0.000	0.000E+01	0.000E+01	0.170E+28	0.193E+28	0.000E+01
343.0	0.000	0.000E+01	0.000E+01	0.104E+28	0.962E+27	0.000E+01
345.0	0.000	0.000E+01	0.000E+01	0.774E+27	0.104E+28	0.000E+01
380.0	0.000	0.000E+01	0.000E+01	0.177E+28	0.198E+28	0.000E+01
454.0	0.000	0.000E+01	0.000E+01	0.235E+28	0.237E+28	0.000E+01
454.3	0.000	0.000E+01	0.000E+01	0.499E+28	0.895E+28	0.000E+01

R calculated using lobe spectral indices from (2)

P_{5000} : 'Refs1' fluxes, (2) spectral indices

P_{5000} : 'refs1' fluxes, s.i. = 0.8

P_{5000} : (2) fluxes & SI

P_{5000} : (2) fluxes, SI = 0.8

P_{5000} extended : (2) spectral indices (REF1 - REF5 2) fluxes

H0=50 OMEGA=1

3C R P5000 SI	Z HF	REF1,HF	REF1,.8	LP,HF	LP, .8	EXT,HF
CLASSICAL DOUBLES						
9.0	0.000	0.114E+28	0.859E+27	0.131E+28	0.984E+27	0.114E+28
47.0	0.058	0.763E+26	0.723E+26	0.784E+26	0.744E+26	0.705E+26
175.0	0.035	0.179E+27	0.157E+27	0.174E+27	0.153E+27	0.169E+27
190.0	0.000	0.528E+27	0.496E+27	0.516E+27	0.484E+27	0.528E+27
191.0	0.000	0.126E+28	0.995E+27	0.984E+27	0.776E+27	0.126E+28
196.0	0.000	0.147E+28	0.138E+28	0.141E+28	0.132E+28	0.147E+28
204.0	0.050	0.252E+27	0.205E+27	0.214E+27	0.174E+27	0.227E+27
205.0	0.017	0.859E+27	0.727E+27	0.799E+27	0.676E+27	0.823E+27
207.0	0.525	0.200E+27	0.228E+27	0.231E+27	0.263E+27	0.118E+27
208.0	0.042	0.396E+27	0.296E+27	0.368E+27	0.275E+27	0.361E+27
212.0	0.250	0.463E+27	0.443E+27	0.416E+27	0.398E+27	0.316E+27
215.0	0.045	0.228E+26	0.210E+26	0.283E+26	0.261E+26	0.214E+26
249.1	0.152	0.248E+26	0.247E+26	0.280E+26	0.279E+26	0.208E+26
254.0	0.014	0.202E+27	0.177E+27	0.190E+27	0.167E+27	0.197E+27
263.0	0.094	0.178E+27	0.174E+27	0.178E+27	0.174E+27	0.156E+27
268.4	0.032	0.699E+27	0.607E+27	0.574E+27	0.499E+27	0.651E+27
270.1	0.060	0.172E+28	0.152E+28	0.959E+27	0.850E+27	0.150E+28
275.1	0.075	0.168E+27	0.159E+27	0.114E+27	0.108E+27	0.150E+27
325.0	0.003	0.524E+27	0.450E+27	0.391E+27	0.335E+27	0.500E+27
334.0	0.208	0.895E+26	0.856E+26	0.708E+26	0.678E+26	0.684E+26
351.0	0.010	0.639E+26	0.643E+26	0.614E+26	0.618E+26	0.629E+26
245.0	1.854	0.639E+27	0.695E+27	0.551E+27	0.600E+27	0.160E+27
455.0	0.370	0.101E+27	0.954E+26	0.111E+27	0.105E+27	0.652E+26
DOUBLES WITHOUT CENTRAL COMPONENTS						
14.0	0.000	0.286E+27	0.262E+27	0.273E+27	0.250E+27	0.286E+27
68.1	0.000	0.548E+27	0.513E+27	0.561E+27	0.526E+27	0.548E+27
181.0	0.000	0.713E+27	0.648E+27	0.588E+27	0.534E+27	0.713E+27
336.0	0.000	0.292E+27	0.265E+27	0.265E+27	0.241E+27	0.292E+27
16.5	0.000	0.940E+26	0.164E+27	0.000E+01	0.000E+01	0.940E+26
432.0	0.000	0.331E+28	0.250E+28	0.583E+27	0.441E+27	0.331E+28
COMPACT QUASARS						
43.0	0.000	0.000E+01	0.000E+01	0.926E+27	0.978E+27	0.000E+01
48.0	0.000	0.000E+01	0.000E+01	0.271E+27	0.268E+27	0.000E+01
138.0	0.000	0.000E+01	0.000E+01	0.835E+27	0.946E+27	0.000E+01
147.0	0.000	0.000E+01	0.000E+01	0.918E+27	0.930E+27	0.000E+01
186.0	0.000	0.000E+01	0.000E+01	0.225E+27	0.177E+27	0.000E+01
216.0	0.000	0.000E+01	0.000E+01	0.295E+27	0.315E+27	0.000E+01
287.0	0.000	0.000E+01	0.000E+01	0.127E+28	0.148E+28	0.000E+01
286.0	0.000	0.000E+01	0.000E+01	0.180E+28	0.215E+28	0.000E+01
309.1	0.000	0.000E+01	0.000E+01	0.108E+28	0.123E+28	0.000E+01
343.0	0.000	0.000E+01	0.000E+01	0.637E+27	0.590E+27	0.000E+01
345.0	0.000	0.000E+01	0.000E+01	0.573E+27	0.769E+27	0.000E+01
380.0	0.000	0.000E+01	0.000E+01	0.125E+28	0.140E+28	0.000E+01
454.0	0.000	0.000E+01	0.000E+01	0.104E+28	0.105E+28	0.000E+01
454.3	0.000	0.000E+01	0.000E+01	0.325E+28	0.583E+28	0.000E+01

H0=100 OMEGA=0

3C R P5000

SI	HF	REF1/HF	REF1/.8	LP/HF	LP/.8	EXT/HF
CLASSICAL DOUBLES						
9.0	0.000	0.715E+27	0.537E+27	0.819E+27	0.615E+27	0.715E+27
47.0	0.058	0.237E+26	0.224E+26	0.243E+26	0.231E+26	0.219E+26
175.0	0.035	0.659E+26	0.578E+26	0.639E+26	0.561E+26	0.620E+26
190.0	0.000	0.237E+27	0.222E+27	0.231E+27	0.217E+27	0.237E+27
191.0	0.000	0.772E+27	0.609E+27	0.602E+27	0.474E+27	0.772E+27
196.0	0.000	0.565E+27	0.531E+27	0.544E+27	0.511E+27	0.565E+27
204.0	0.050	0.109E+27	0.883E+26	0.925E+26	0.750E+26	0.979E+26
205.0	0.017	0.444E+27	0.376E+27	0.414E+27	0.350E+27	0.426E+27
207.0	0.525	0.707E+26	0.806E+26	0.816E+26	0.929E+26	0.416E+26
208.0	0.042	0.170E+27	0.127E+27	0.159E+27	0.119E+27	0.156E+27
212.0	0.250	0.194E+27	0.186E+27	0.174E+27	0.167E+27	0.133E+27
215.0	0.045	0.703E+25	0.647E+25	0.873E+25	0.804E+25	0.660E+25
249.1	0.152	0.726E+25	0.722E+25	0.821E+25	0.817E+25	0.611E+25
254.0	0.014	0.731E+26	0.641E+26	0.687E+26	0.602E+26	0.713E+26
263.4	0.094	0.620E+26	0.605E+26	0.620E+26	0.605E+26	0.542E+26
268.4	0.032	0.342E+27	0.297E+27	0.281E+27	0.244E+27	0.318E+27
270.1	0.060	0.882E+27	0.783E+27	0.493E+27	0.437E+27	0.774E+27
275.1	0.075	0.557E+26	0.528E+26	0.377E+26	0.357E+26	0.498E+26
325.0	0.003	0.215E+27	0.184E+27	0.160E+27	0.137E+27	0.205E+27
334.0	0.208	0.296E+26	0.284E+26	0.235E+26	0.224E+26	0.226E+26
351.0	0.010	0.193E+26	0.194E+26	0.185E+26	0.187E+26	0.190E+26
245.0	1.854	0.265E+27	0.289E+27	0.229E+27	0.249E+27	0.663E+26
455.0	0.370	0.334E+26	0.314E+26	0.366E+26	0.344E+26	0.215E+26
DOUBLES WITHOUT CENTRAL COMPONENTS						
14.0	0.000	0.117E+27	0.107E+27	0.112E+27	0.102E+27	0.117E+27
68.1	0.000	0.250E+27	0.234E+27	0.256E+27	0.240E+27	0.250E+27
181.0	0.000	0.346E+27	0.314E+27	0.285E+27	0.259E+27	0.346E+27
336.0	0.000	0.116E+27	0.105E+27	0.105E+27	0.953E+26	0.116E+27
16.5	0.000	0.385E+26	0.671E+26	0.000E+01	0.000E+01	0.385E+26
432.0	0.000	0.191E+28	0.145E+28	0.336E+27	0.255E+27	0.191E+28
COMPACT QUASARS						
43.0	0.000	0.000E+01	0.000E+01	0.464E+27	0.490E+27	0.000E+01
48.0	0.000	0.000E+01	0.000E+01	0.816E+26	0.808E+26	0.000E+01
138.0	0.000	0.000E+01	0.000E+01	0.306E+27	0.346E+27	0.000E+01
147.0	0.000	0.000E+01	0.000E+01	0.302E+27	0.306E+27	0.000E+01
186.0	0.000	0.000E+01	0.000E+01	0.947E+26	0.746E+26	0.000E+01
216.0	0.000	0.000E+01	0.000E+01	0.103E+27	0.110E+27	0.000E+01
287.0	0.000	0.000E+01	0.000E+01	0.532E+27	0.623E+27	0.000E+01
286.0	0.000	0.000E+01	0.000E+01	0.688E+27	0.822E+27	0.000E+01
309.1	0.000	0.000E+01	0.000E+01	0.425E+27	0.484E+27	0.000E+01
343.0	0.000	0.000E+01	0.000E+01	0.259E+27	0.241E+27	0.000E+01
345.0	0.000	0.000E+01	0.000E+01	0.194E+27	0.260E+27	0.000E+01
380.0	0.000	0.000E+01	0.000E+01	0.442E+27	0.496E+27	0.000E+01
454.0	0.000	0.000E+01	0.000E+01	0.588E+27	0.594E+27	0.000E+01
454.3	0.000	0.000E+01	0.000E+01	0.125E+28	0.224E+28	0.000E+01

END OF PRINT: JCM T014 SPQR0044 D_PR1

HO=100 OMEGA=1

3C R P5000

SI	; HF	REF1,HF	REF1,.8	LP,HF	LP, .8	EXT,HF
		CLASSICAL DOUBLES				
9.0	0.000	0.286E+27	0.215E+27	0.328E+27	0.246E+27	0.286E+27
47.0	0.058	0.191E+26	0.181E+26	0.196E+26	0.186E+26	0.176E+26
175.0	0.035	0.448E+26	0.393E+26	0.435E+26	0.381E+26	0.422E+26
190.0	0.000	0.132E+27	0.124E+27	0.129E+27	0.121E+27	0.132E+27
191.0	0.000	0.316E+27	0.249E+27	0.246E+27	0.194E+27	0.316E+27
196.0	0.000	0.366E+27	0.344E+27	0.352E+27	0.331E+27	0.366E+27
204.0	0.050	0.631E+26	0.512E+26	0.536E+26	0.435E+26	0.568E+26
205.0	0.017	0.215E+27	0.182E+27	0.200E+27	0.169E+27	0.206E+27
207.0	0.525	0.501E+26	0.571E+26	0.578E+26	0.658E+26	0.295E+26
208.0	0.042	0.989E+26	0.739E+26	0.921E+26	0.688E+26	0.904E+26
212.0	0.250	0.116E+27	0.111E+27	0.104E+27	0.995E+26	0.791E+26
215.0	0.045	0.570E+25	0.525E+25	0.709E+25	0.652E+25	0.536E+25
249.1	0.152	0.620E+25	0.617E+25	0.701E+25	0.697E+25	0.521E+25
254.0	0.014	0.506E+26	0.443E+26	0.475E+26	0.416E+26	0.493E+26
263.0	0.094	0.445E+26	0.434E+26	0.445E+26	0.434E+26	0.389E+26
268.4	0.032	0.175E+27	0.152E+27	0.144E+27	0.125E+27	0.163E+27
270.1	0.060	0.429E+27	0.381E+27	0.240E+27	0.213E+27	0.376E+27
275.1	0.075	0.420E+26	0.398E+26	0.284E+26	0.270E+26	0.376E+26
325.0	0.003	0.131E+27	0.112E+27	0.977E+26	0.839E+26	0.125E+27
334.0	0.208	0.224E+26	0.214E+26	0.177E+26	0.169E+26	0.171E+26
351.0	0.010	0.160E+26	0.161E+26	0.153E+26	0.154E+26	0.157E+26
245.0	1.854	0.160E+27	0.174E+27	0.138E+27	0.150E+27	0.399E+26
455.0	0.370	0.254E+26	0.239E+26	0.278E+26	0.261E+26	0.163E+26
		DOUBLES WITHOUT CENTRAL COMPONENTS				
14.0	0.000	0.716E+26	0.654E+26	0.683E+26	0.624E+26	0.716E+26
68.1	0.000	0.137E+27	0.128E+27	0.140E+27	0.132E+27	0.137E+27
181.0	0.000	0.178E+27	0.162E+27	0.147E+27	0.134E+27	0.178E+27
336.0	0.000	0.731E+26	0.662E+26	0.664E+26	0.601E+26	0.731E+26
16.5	0.000	0.235E+26	0.409E+26	0.000E+01	0.000E+01	0.235E+26
432.0	0.000	0.827E+27	0.626E+27	0.146E+27	0.110E+27	0.827E+27
		COMPACT QUASARS				
43.0	0.000	0.000E+01	0.000E+01	0.232E+27	0.244E+27	0.000E+01
48.0	0.000	0.000E+01	0.000E+01	0.677E+26	0.671E+26	0.000E+01
138.0	0.000	0.000E+01	0.000E+01	0.209E+27	0.236E+27	0.000E+01
147.0	0.000	0.000E+01	0.000E+01	0.229E+27	0.232E+27	0.000E+01
186.0	0.000	0.000E+01	0.000E+01	0.561E+26	0.442E+26	0.000E+01
216.0	0.000	0.000E+01	0.000E+01	0.738E+26	0.788E+26	0.000E+01
287.0	0.000	0.000E+01	0.000E+01	0.317E+27	0.371E+27	0.000E+01
286.0	0.000	0.000E+01	0.000E+01	0.450E+27	0.538E+27	0.000E+01
309.1	0.000	0.000E+01	0.000E+01	0.271E+27	0.308E+27	0.000E+01
343.0	0.000	0.000E+01	0.000E+01	0.159E+27	0.148E+27	0.000E+01
345.0	0.000	0.000E+01	0.000E+01	0.143E+27	0.192E+27	0.000E+01
380.0	0.000	0.000E+01	0.000E+01	0.312E+27	0.350E+27	0.000E+01
454.0	0.000	0.000E+01	0.000E+01	0.259E+27	0.262E+27	0.000E+01
454.3	0.000	0.000E+01	0.000E+01	0.813E+27	0.146E+28	0.000E+01

Table 4

Observed cumulative distn' $F_n(x)$	Predicted $F(x) = x$		
	$\gamma=2\ \lambda=4$	$\gamma=5\ \lambda=0.25$	$\gamma=10\ \lambda=0.032$
0.07	0.18	0.14	0.16
0.13	0.24	0.20	0.21
0.20	0.32	0.28	0.28
0.27	0.37	0.32	0.32
0.33	0.39	0.34	0.34
0.40	0.39	0.34	0.34
0.47	0.43	0.37	0.37
0.53	0.47	0.41	0.41
0.60	0.51	0.45	0.45
0.67	0.61	0.53	0.53
0.73	0.67	0.59	0.58
0.80	0.70	0.62	0.61
0.87	0.76	0.67	0.66
0.93	[0.78]	[0.69]	[0.68]
1.00	0.91	0.81	0.79

D_n = 0.15 0.24 0.25

$\sqrt{n}\, D_n$ = 0.58 0.93 0.97

$F_n(x)$ if 12 objects in lower bin

	$\gamma=2\ \lambda=12.4$	$\gamma=5\ \lambda=0.78$
0.44	0.52	0.46
0.48	0.54	0.48
0.52	0.57	0.50
0.56	0.61	0.54
0.59	0.63	0.56
0.63	0.65	0.57
0.67	0.65	0.57
0.70	0.67	0.59
0.74	0.69	0.61
0.78	0.72	0.63
0.81	0.78	0.69
0.85	0.83	0.73
0.89	0.84	0.75
0.93	0.88	0.78
0.96	[0.90]	[0.79]
1.00	0.99	0.87

$D_n = 0.08$

D_n = ~~0.06~~ 0.17

$\sqrt{n}\, D_n$ = 0.38 0.66

F_n if 6 objects in lower bin	$\gamma=2\ \lambda=12.4$	$\gamma=5\ \lambda=078$	$D_n=023$	$D_n=0.17$
0.29	0.52	0.46		
033	0.54	0.48	~~$D_n=0.21$ ($\gamma=2$)~~	
0.38	0.57	0.50		
0.43	0.61	0.54		
0.48	0.63	0.56		
0.52	0.65	0.57		
0.57	0.65	0.57		
0.62	0.67	0.59		
0.67	0.69	0.61		
0.71	0.72	0.63		
0.76	0.78	0.69		
0.81	0.83	0.73		
0.86	0.84	0.75		
0.90	0.88	0.78		
0.95	0.90	0.79		~~$D_n=0.16$ ($\gamma=5$)~~
1.00	0.99	0.87		
			$\sqrt{n}\,D_n=0.89$	$\sqrt{n}\,D_n=0.68$

Fig. 1

DOUBLES
-COMPACT
NUMBER
REDSHIFT
(*10.0** -1)
0
10
20
30
40
50
60
70
0
2
4
6
8
10
12
14
16
18
20
22

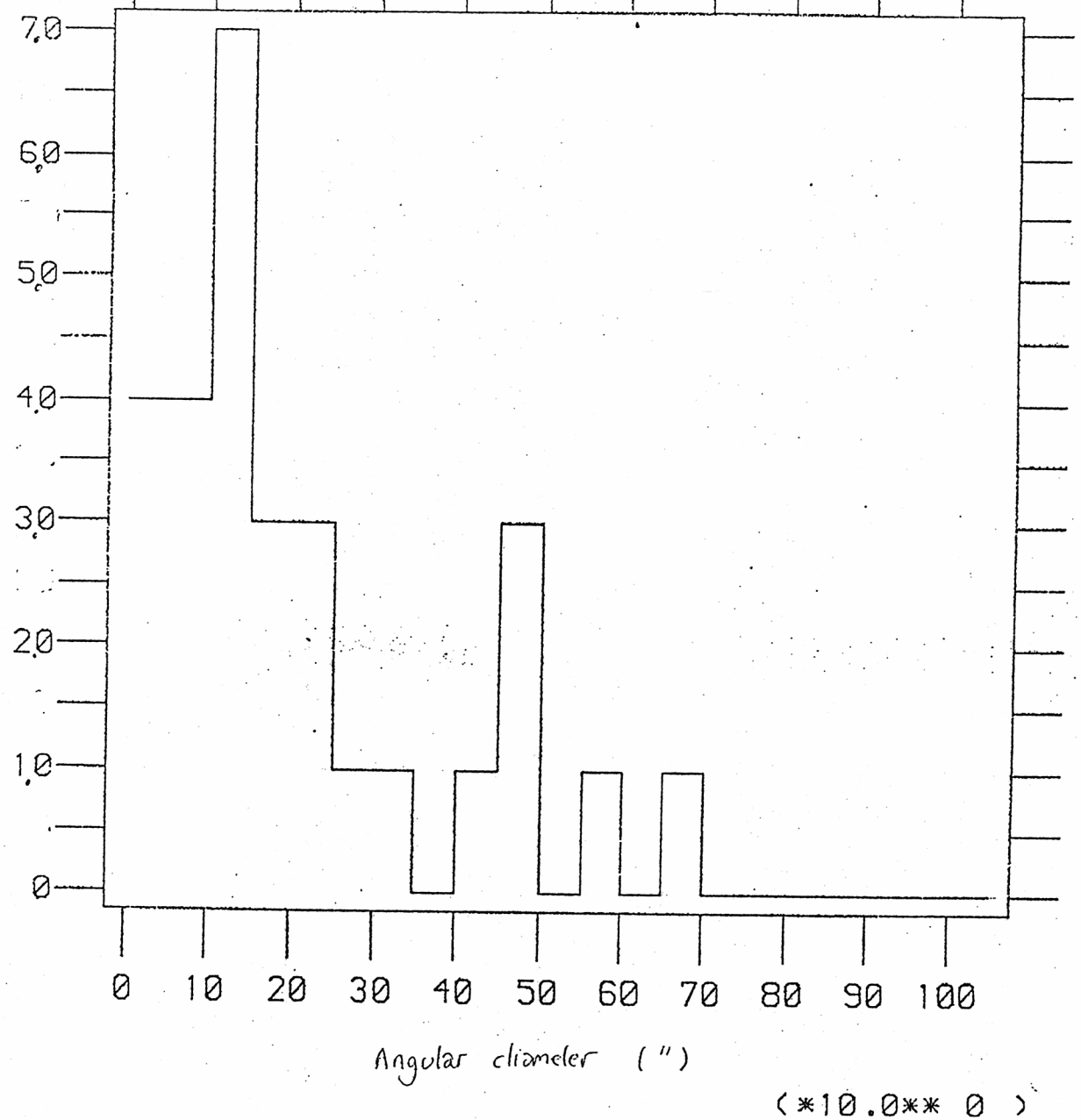
7.0
6.0
5.0
4.0
3.0
2.0
1.0
0
0 10 20 30 40 50 60 70 80 90 100
Angular diameter (")
(*10.0** 0)

Fig. 2

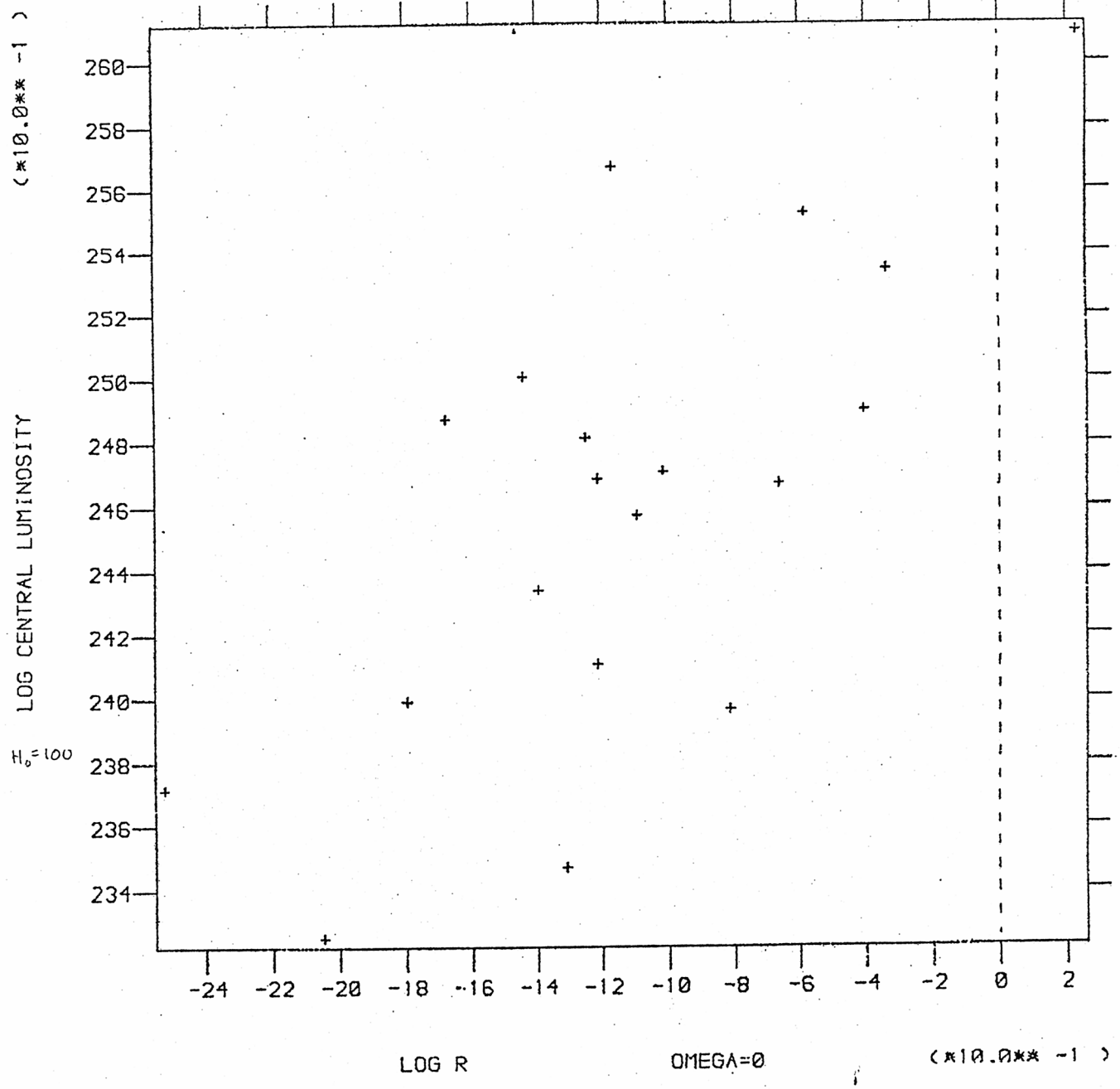
(*10.0** -1)
260
258
256
254
252
250
248
246
244
242
240
238
236
234
LOG CENTRAL LUMINOSITY
$H_0 = 100$
-24
-22
-20
-18
-16
-14
-12
-10
-8
-6
-4
-2
0
2
LOG R
OMEGA=0
(*10.0** -1)

Fig 3 (a)

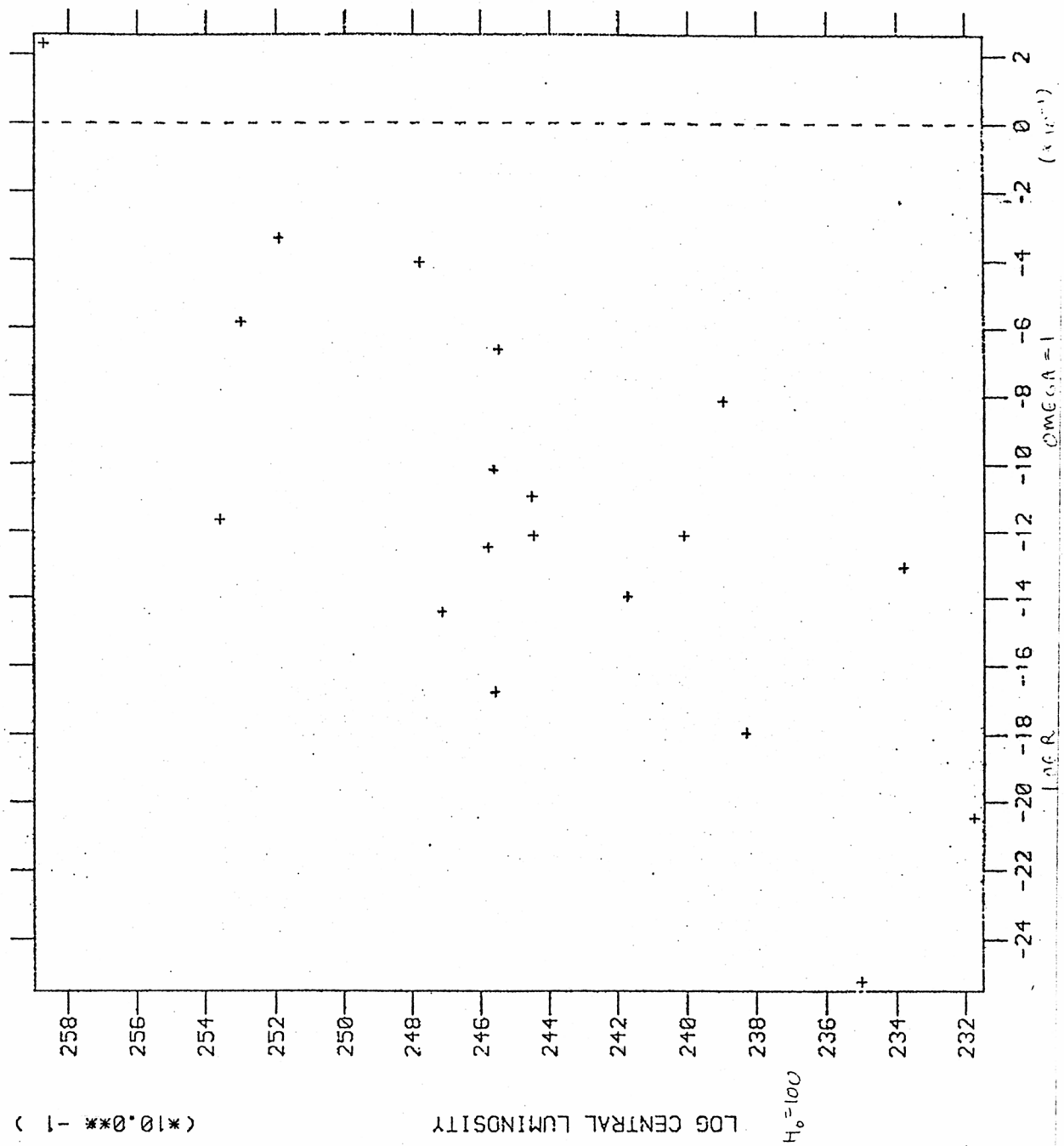
LOG CENTRAL LUMINOSITY
(*10.0** -1)
H_o=100
258
256
254
252
250
248
246
244
242
240
238
236
234
232
2
0
-2
-4
-6
-8
-10
-12
-14
-16
-18
-20
-22
-24
OMEGA=1
LOG R

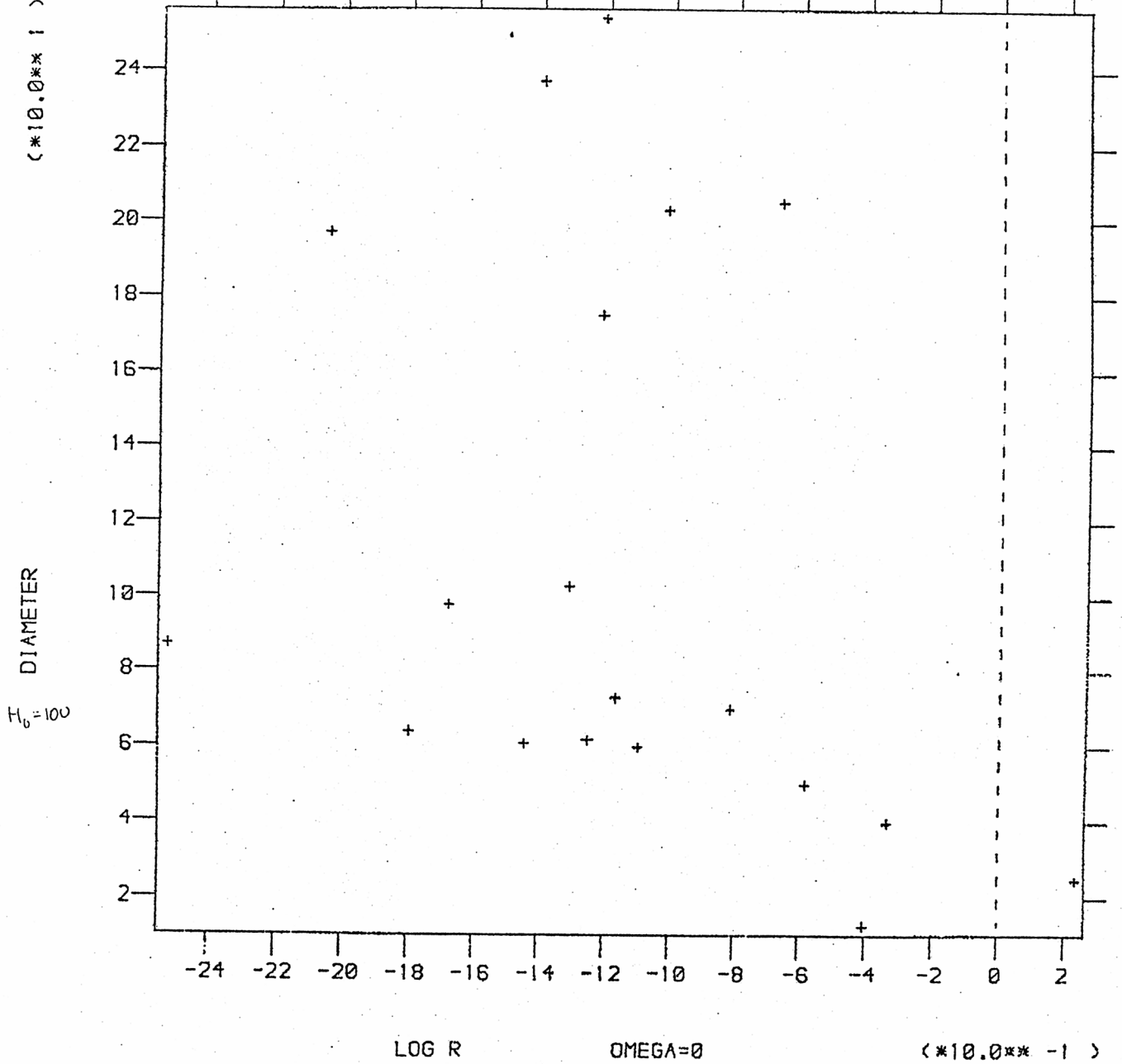
(*10.0** 1)
24
22
20
18
16
14
12
10
8
6
4
2
DIAMETER
H_0=100
-24 -22 -20 -18 -16 -14 -12 -10 -8 -6 -4 -2 0 2
LOG R
OMEGA=0
(*10.0** -1)

Fig 4 (a)

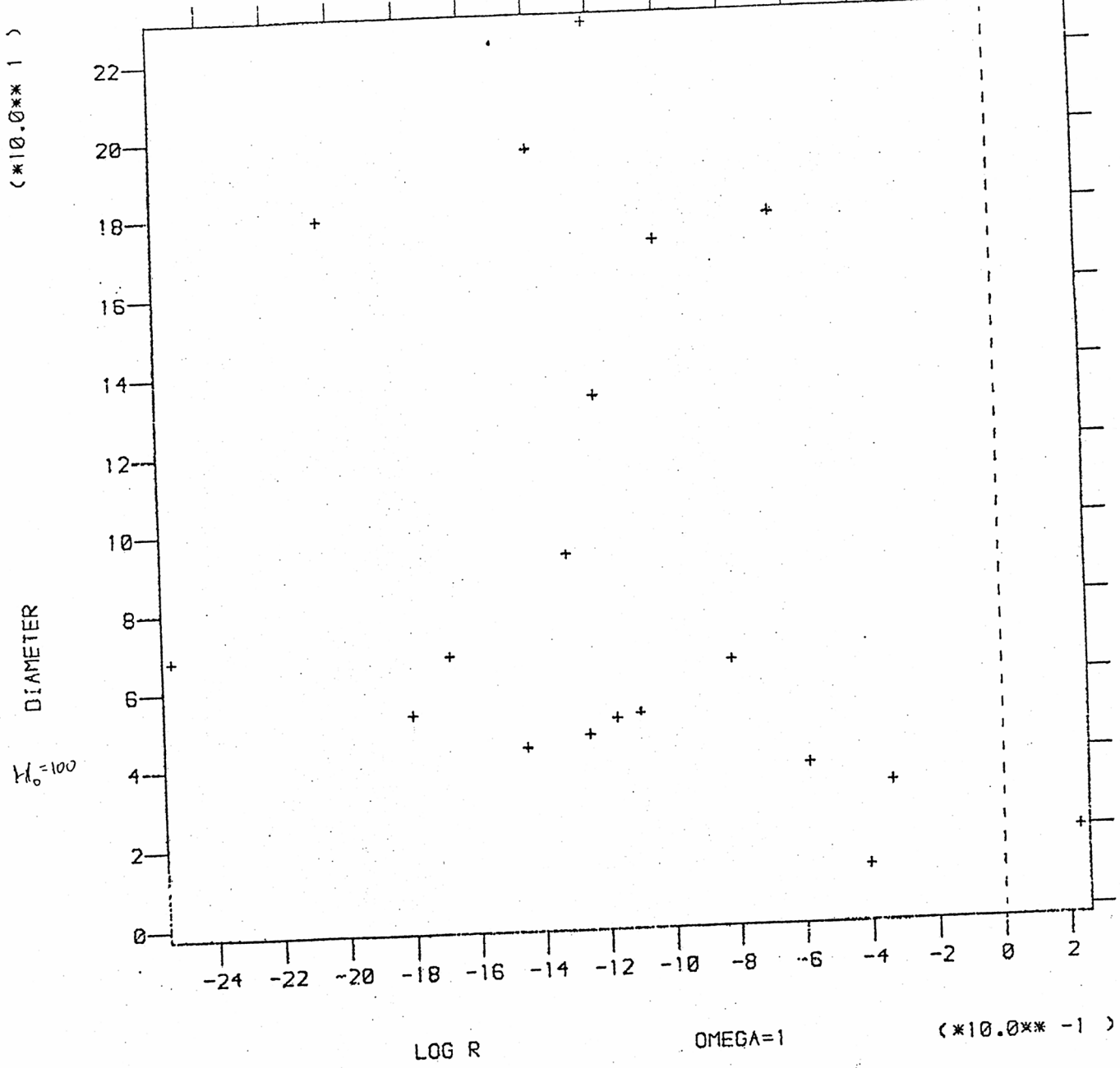
(*10.0** 1)
22
20
18
16
14
12
10
8
6
4
2
0
DIAMETER
H_0=100
-24 -22 -20 -18 -16 -14 -12 -10 -8 -6 -4 -2 0 2
LOG R
OMEGA=1
(*10.0** -1)

Fig 4(a)

Fig 5(a)

NUMBER
(*10.0** 0
0
1
2
3
4
5
6
7
8
9
10
11
0 5 10 15 20 25 30 35 40 45 50 55 60
DIAMETER
H_0=100 Ω_J=0
(*10.0** 1)

Fig 5 (b)

NUMBER
(*10.0** 0
0
1
2
3
4
5
6
7
8
9
10
0 5 10 15 20 25 30 35 40 45 50 55 60
DIAMETER
$\mu_0 = 100$ $\Omega = 1$
(*10.0** 1)

Fig 5(c)

NUMBER
(*10.0** 1)
0
10
20
30
40
50
60
70
80
0 5 10 15 20 25 30 35 40 45 50 55 60
DIAMETER
μ_0=50 Ω=0

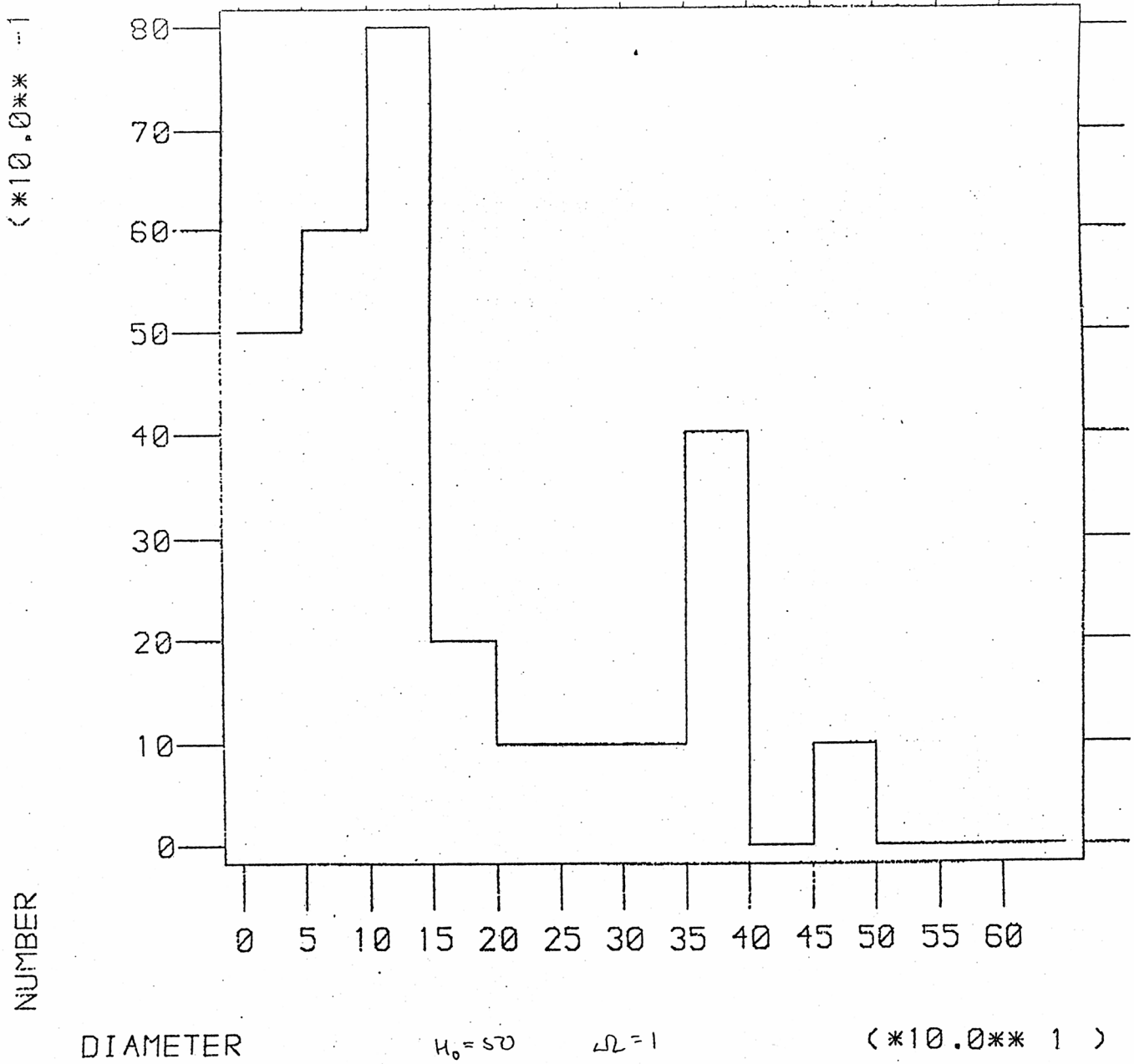
(*10.0** -1
80
70
60
50
40
30
20
10
0
NUMBER
0 5 10 15 20 25 30 35 40 45 50 55 60
DIAMETER
$H_0 = 50$
$\Omega = 1$
(*10.0** 1)

Fig 5(a)

Fig 6

NUMBER
Q
(*10.0** -2)
(*10.0** 0)
0
1
2
3
4
5
6
7
8
9
10
11
12
13
0
5
10
15
20
25
30
35
40
45
50

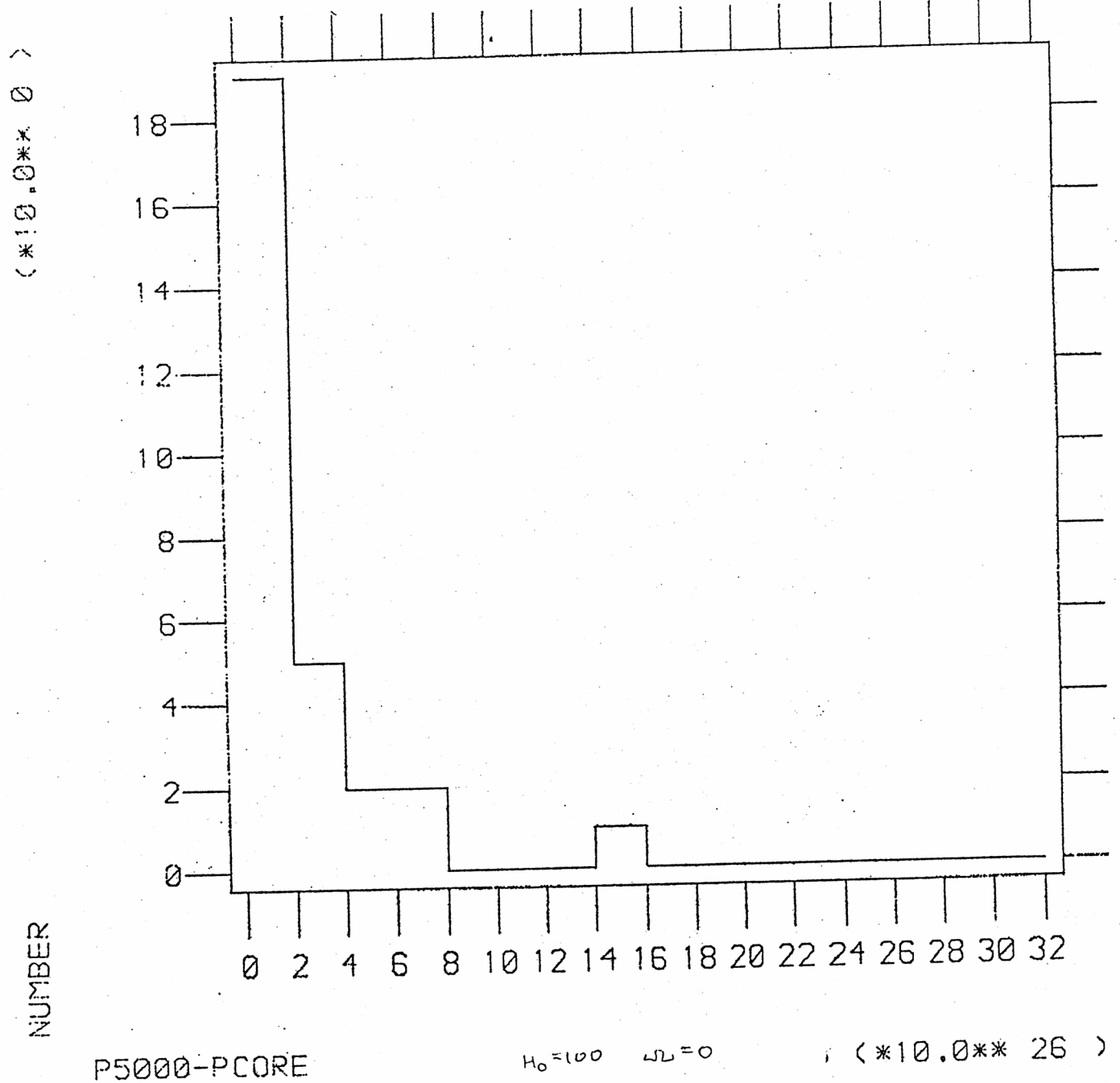
(*10.0** 0)
18
16
14
12
10
8
6
4
2
0
NUMBER
0 2 4 6 8 10 12 14 16 18 20 22 24 26 28 30 32
P5000-PCORE
H_0=100 Ω=0
(*10.0** 26)

Fig 7

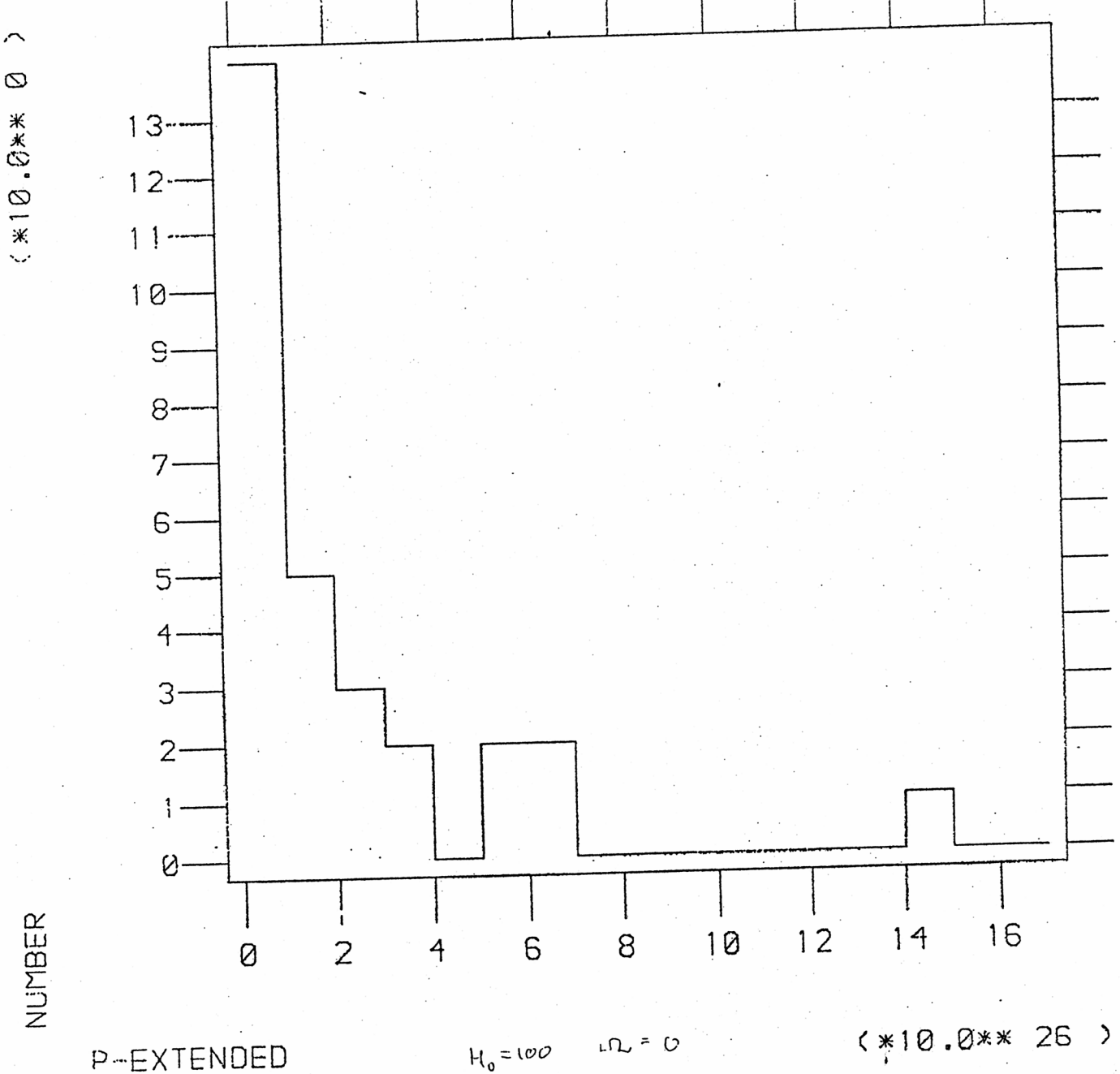
(*10.0** 0)
13
12
11
10
9
8
7
6
5
4
3
2
1
0
NUMBER
0
2
4
6
8
10
12
14
16
P-EXTENDED
$H_0 = 100$
$\Omega = 0$
(*10.0** 26)

Fig 8 (a)

Fig 8 (b)

Fig) (a)

P--CORE
$H_0 = 100$ $\Omega = 0$
(*10.0** 24)
NUMBER
(*10.0** 0)
0
5
10
15
20
25
30
35
40
45
50
0
1
2
3
4
5
6
7
8
9
10
11
12
13
14

NUMBER
P-CORE
(*10.0** 24)
$H_0 = 100$ $\Delta\nu = 1$
(*10.0** 0)

NUMBER
(*10.0** 0
0
1
2
3
4
5
6
7
8
9
10
11
12
0
2
4
6
8
10
12
14
16
18
20
(*10.0** 27)
P-178

Fig 10 (5)

NUMBER
(*10.0** 0)
0
2
4
6
8
10
12
14
16
0
2
4
6
8
10
12
14
16
18
20
(*10.0** 27)
P178 H₀=100 OMEGA=1

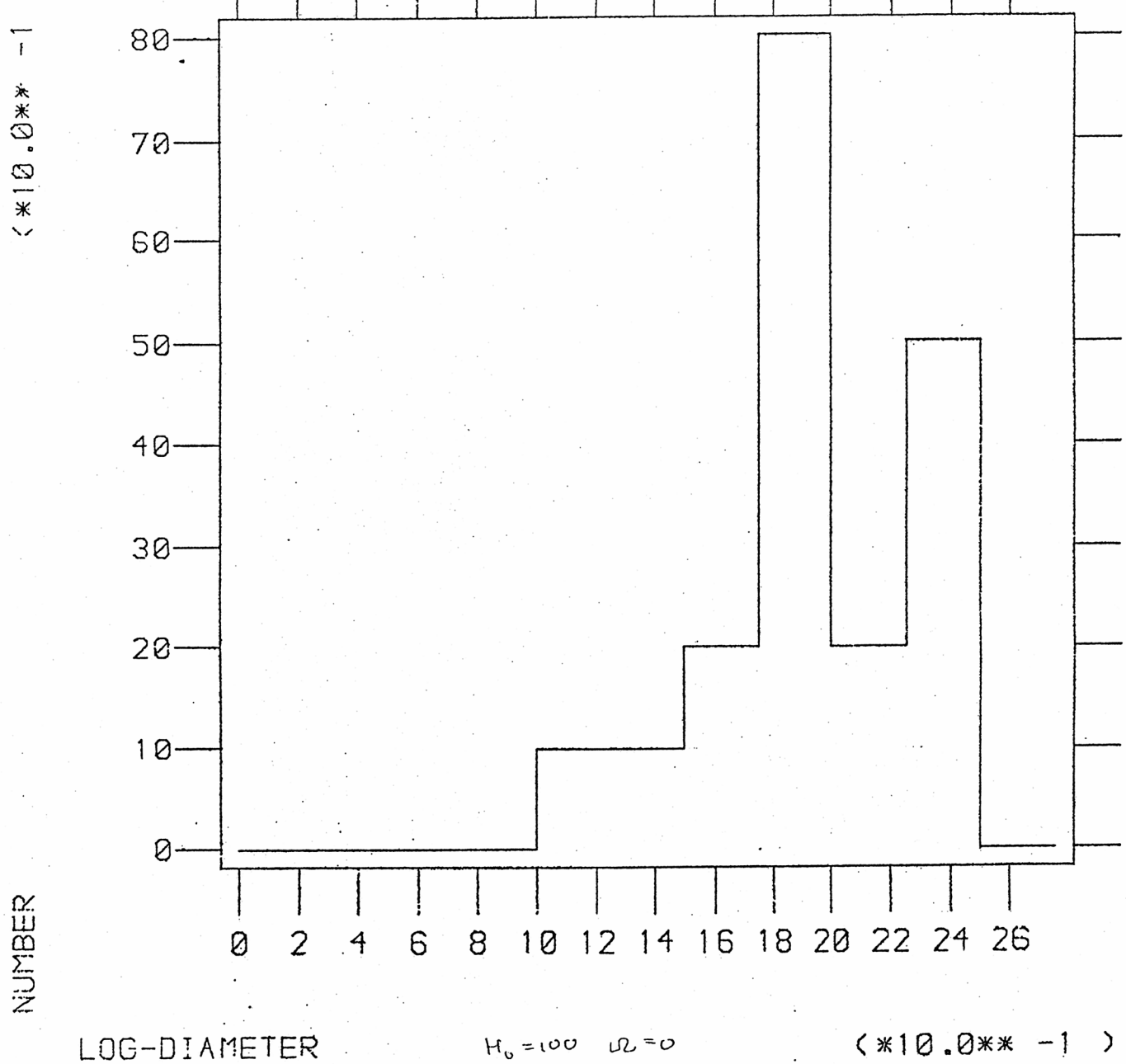
NUMBER
(*10.0** -1)
80
70
60
50
40
30
20
10
0
0 2 4 6 8 10 12 14 16 18 20 22 24 26
LOG-DIAMETER
H_0=100 Ω=0
(*10.0** -1)

Fig 11

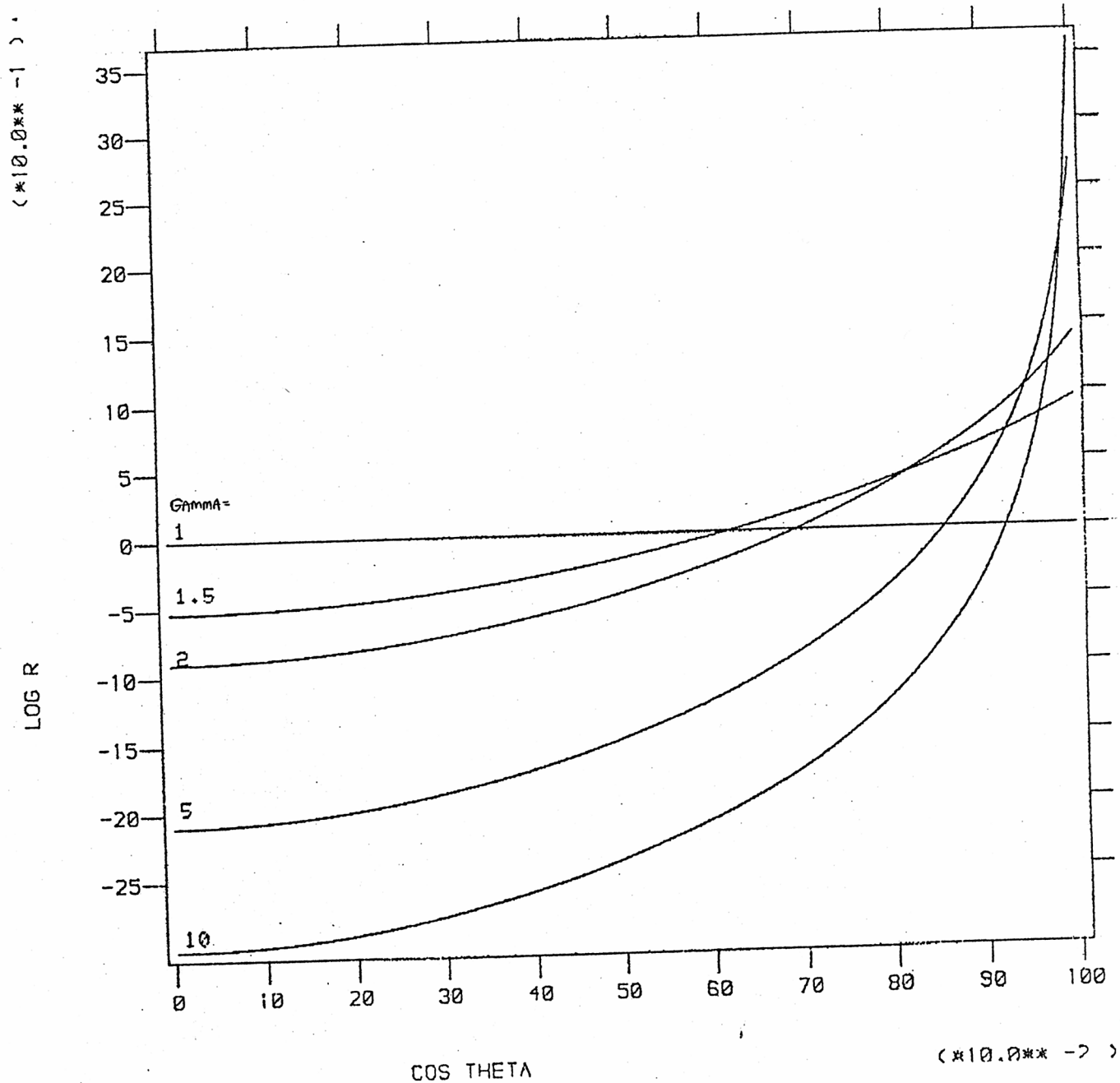
(*10.0** -1)
35
30
25
20
15
10
5
0
-5
-10
-15
-20
-25
GAMMA=
1
1.5
2
5
10
LOG R
0
10
20
30
40
50
60
70
80
90
100
COS THETA
(*10.0** -2)

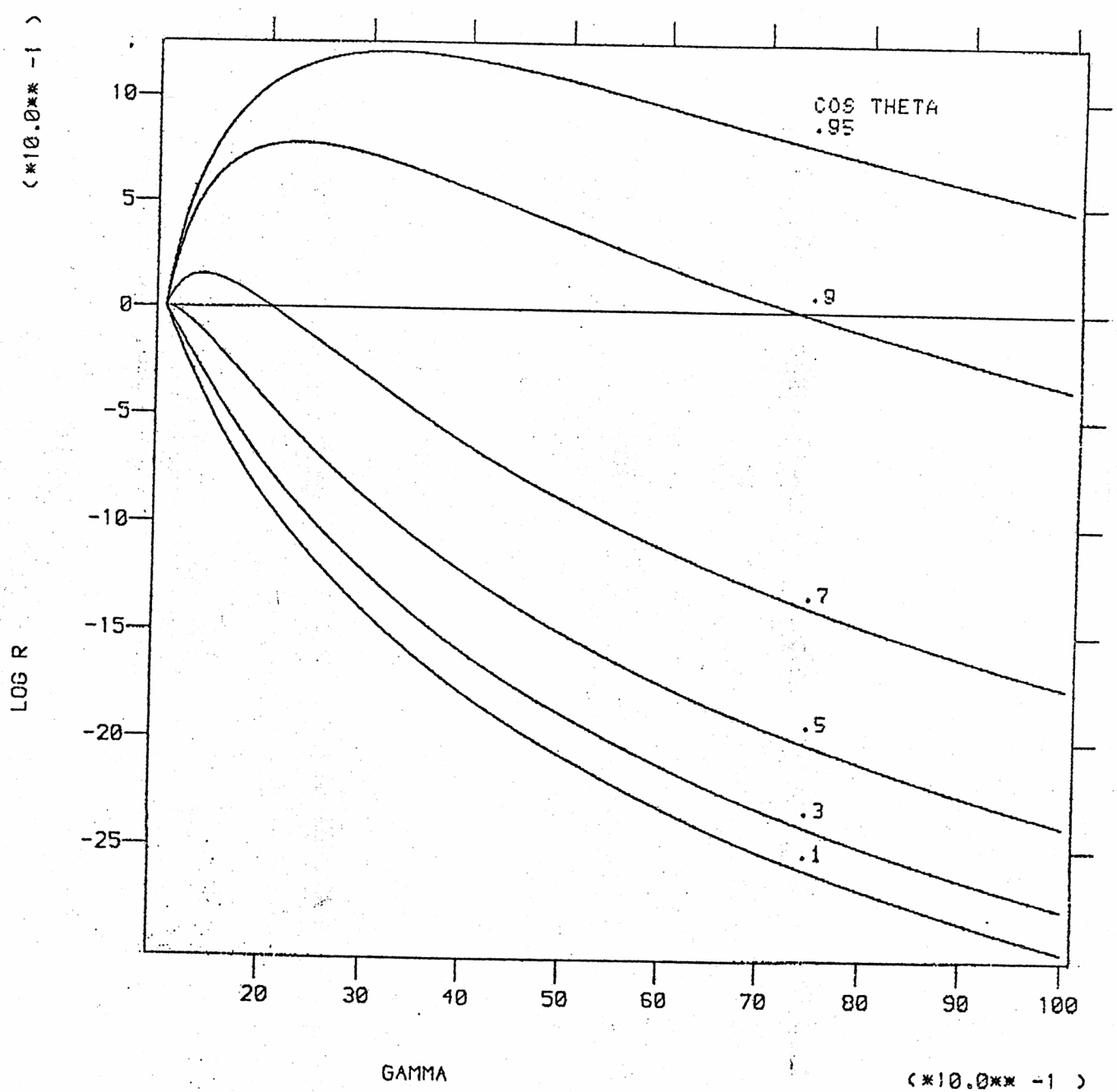
(*10.0** -1)
10
5
0
-5
-10
-15
-20
-25
LOG R
COS THETA
.95
.9
.7
.5
.3
.1
20
30
40
50
60
70
80
90
100
GAMMA
(*10.0** -1)

Fig 13

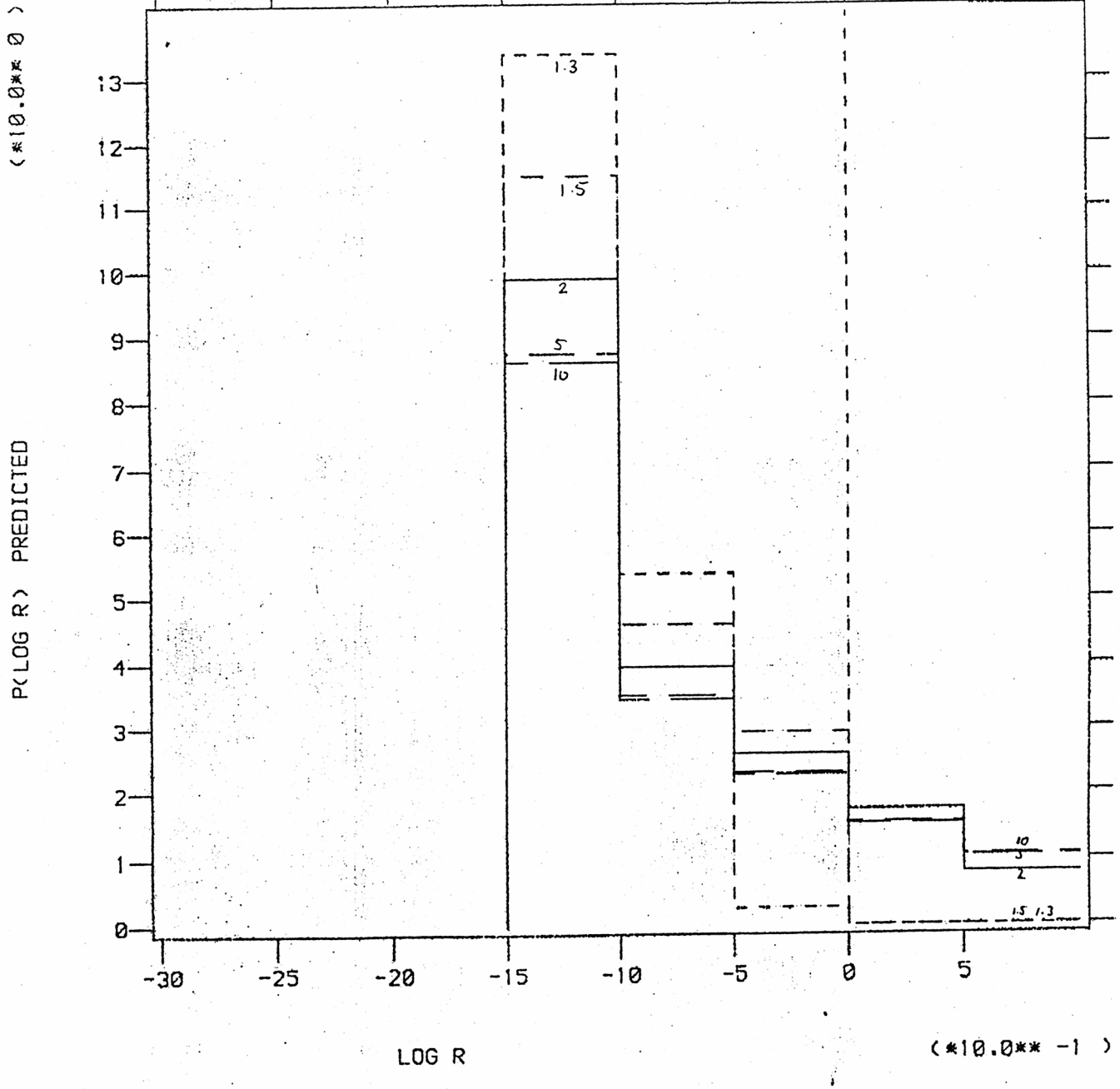
P(LOG R) PREDICTED
(*10.0** 0)
13
12
11
10
9
8
7
6
5
4
3
2
1
0
-30
-25
-20
-15
-10
-5
0
5
LOG R
(*10.0** -1)
1.3
1.5
2
5
10
10
5
2
1.5 1.3

Fig 14

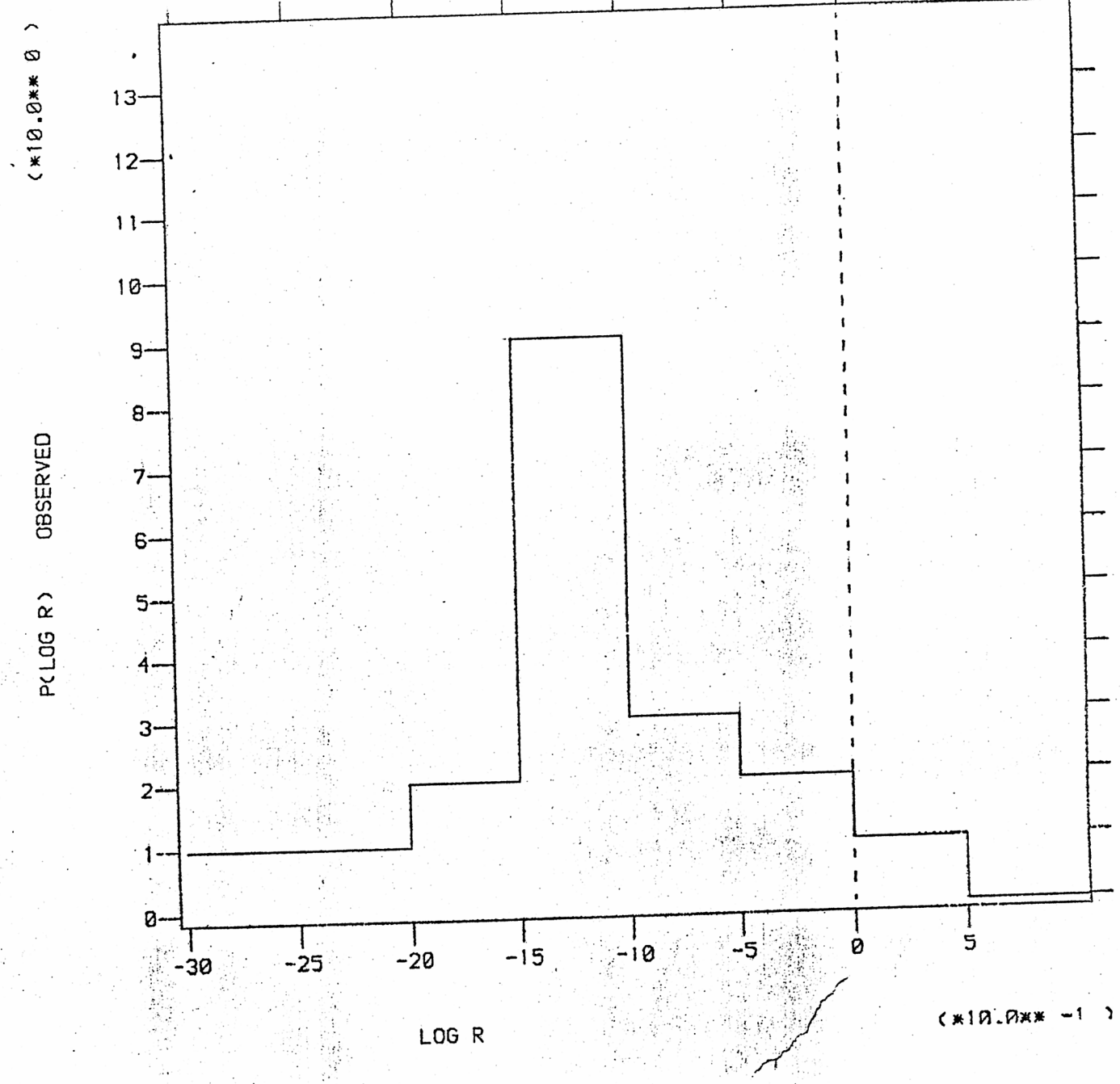
P(LOG R) OBSERVED
(*10.0** 0)
13
12
11
10
9
8
7
6
5
4
3
2
1
0
-30
-25
-20
-15
-10
-5
0
5
LOG R
(*10.0** -1)

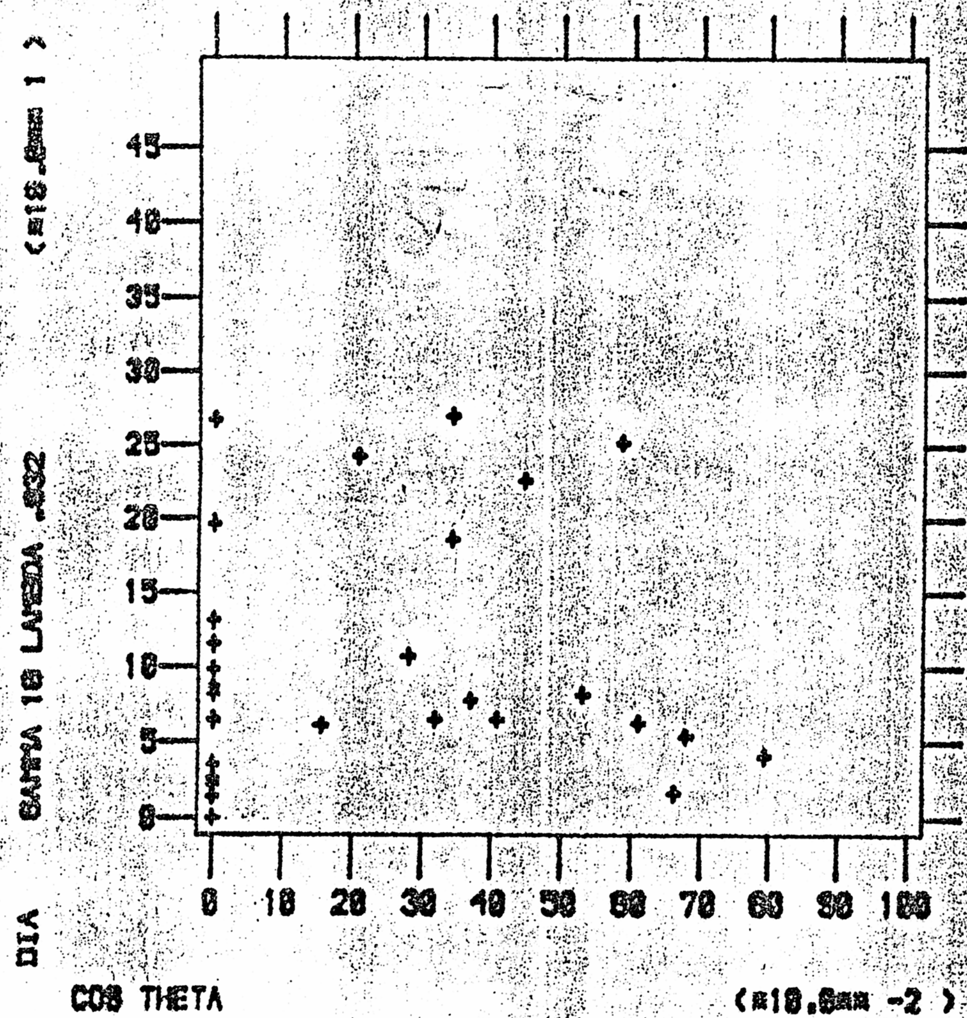

Fig 16(a)

Fig 16(6)

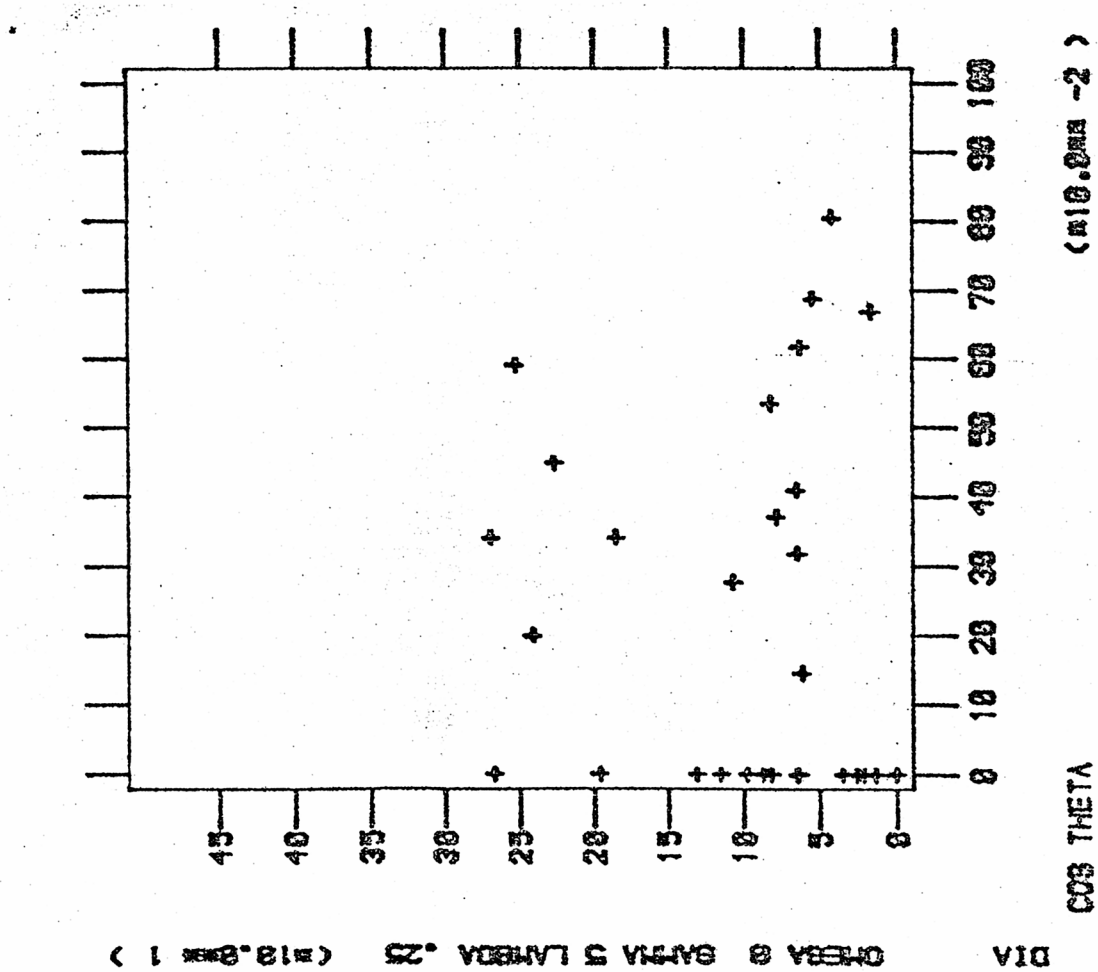
COS THETA
(x10.0mm -2)
0 10 20 30 40 50 60 70 80 90 100
45 40 35 30 25 20 15 10 5 0
DIA
OMEGA 0 GAMMA 5 LAMBDA .25 (=13.8mm)

Fig 16 (c)

45
40
35
30
25
20
15
10
5
0
0 10 20 30 40 50 60 70 80 90 100
COS THETA
(x10.0mm -2)
DIA OMEGA 1 GAMMA 2 LAMBDA 4
(x10.0mm 1)

Fig 16 (d)

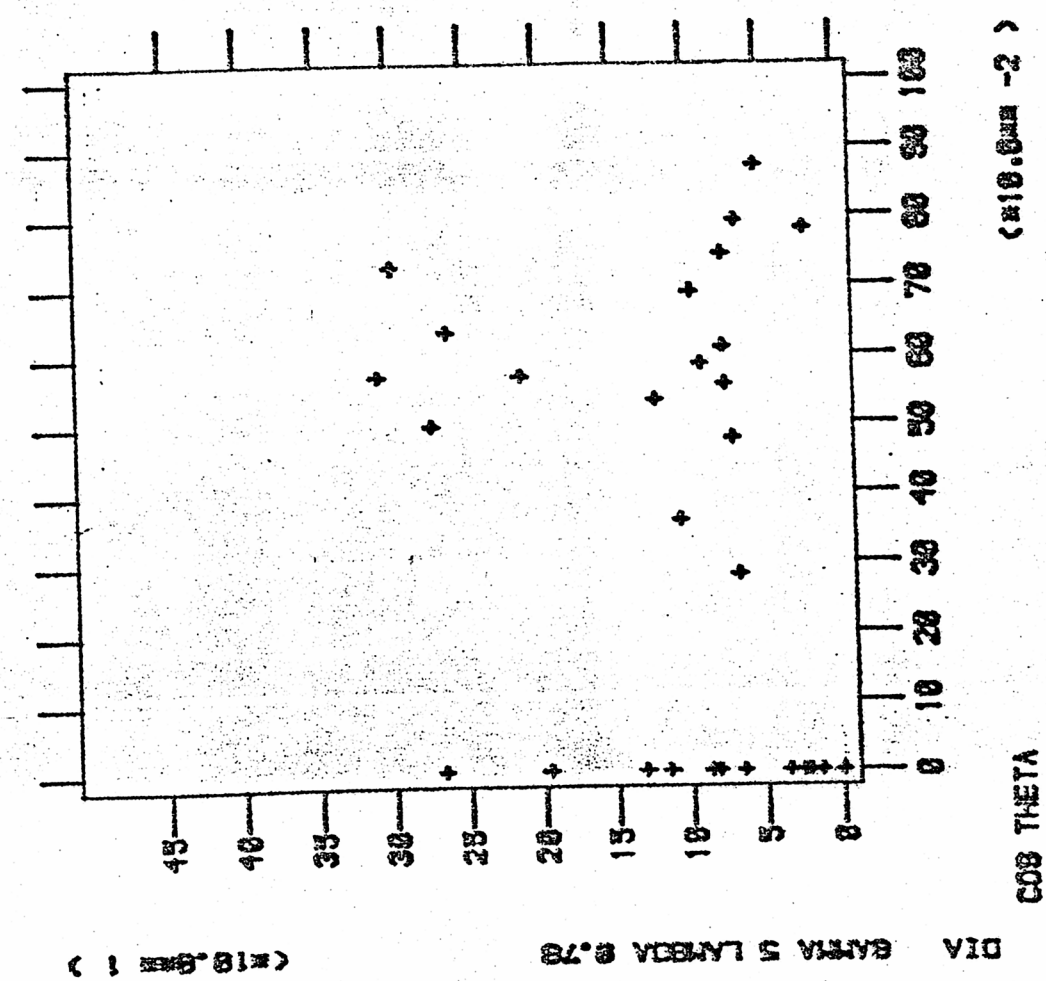
DIA GAMMA 5 LAMBDA 0.78
(x10.0mm -2)
(x10.0mm 1)
COS THETA
0
10
20
30
40
50
60
70
80
90
100
45
40
35
30
25
20
15
10
5
0

Fig 16 (e)

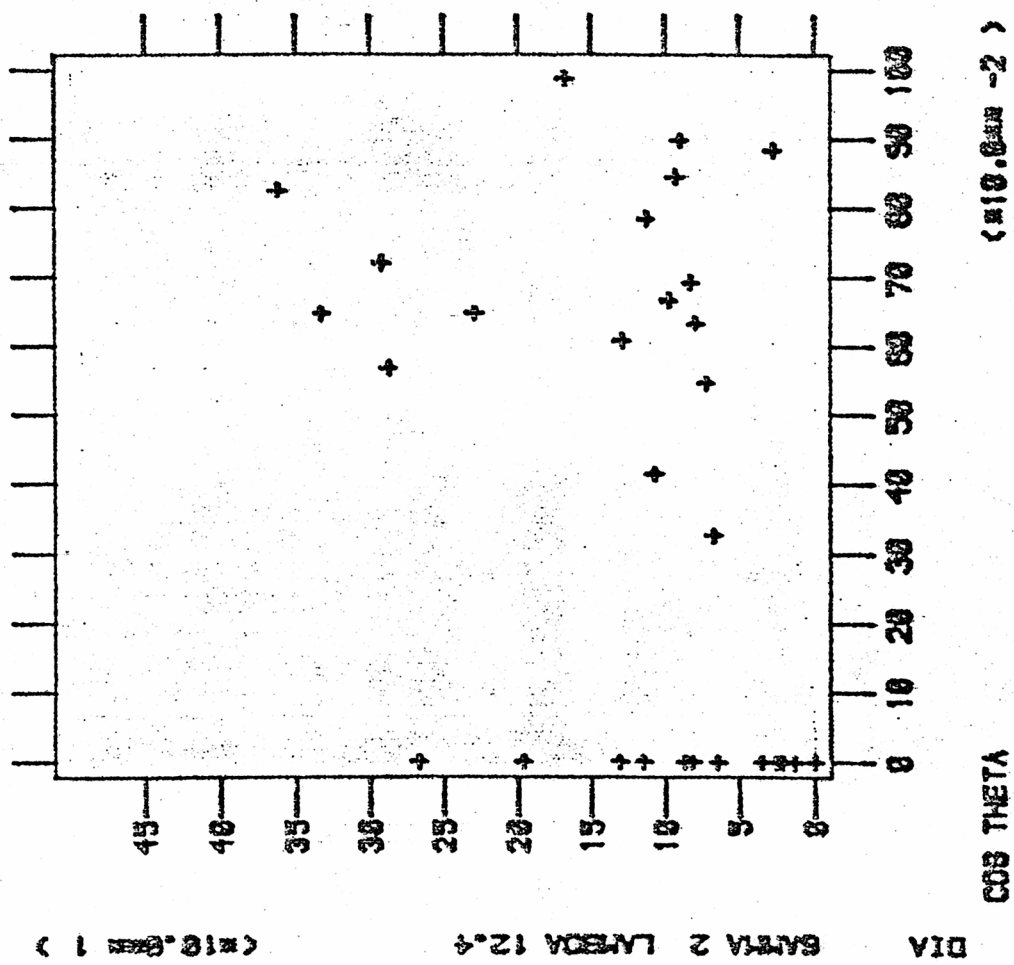
0 10 20 30 40 50 60 70 80 90 100
COS THETA
(*10.0**-2)
45 40 35 30 25 20 15 10 5 0
DIA
BATCH 2 LAMBDA 12.4
(*10.0** 1)

45
40
35
30
25
20
15
10
5
0
0
10
20
30
40
50
60
70
80
90
100
COS THETA
(x10.0mm -2)
(x10.0mm 1)

Fig 16 (g)

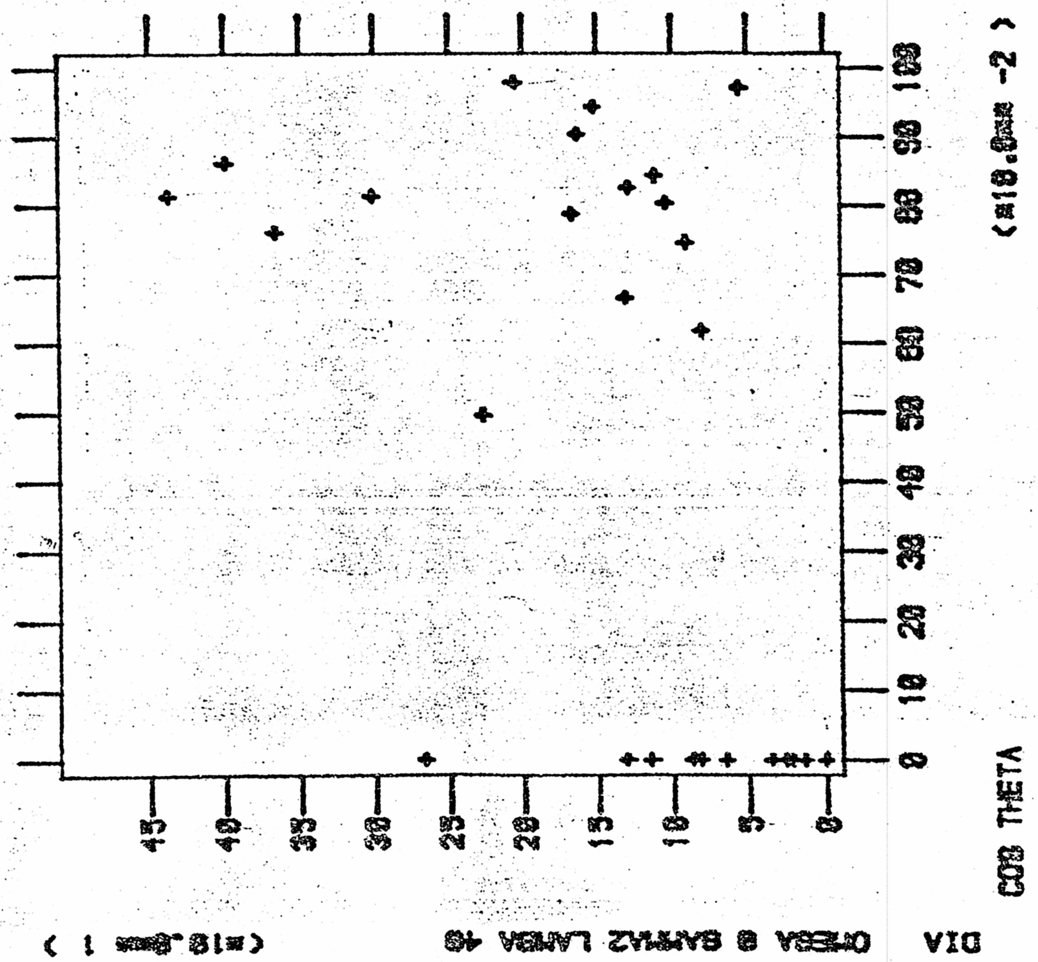

COS THETA
(*10.0** -2)
0
10
20
30
40
50
60
70
80
90
100
0
5
10
15
20
25
30
35
40
45

Fig 16(h)

0
10
20
30
40
50
60
70
80
90
100
COS THETA
45
40
35
30
25
20
15
10
5
0
DIA GAMMA 1.5 LAMBDA 9.4
(*10.0** 1)

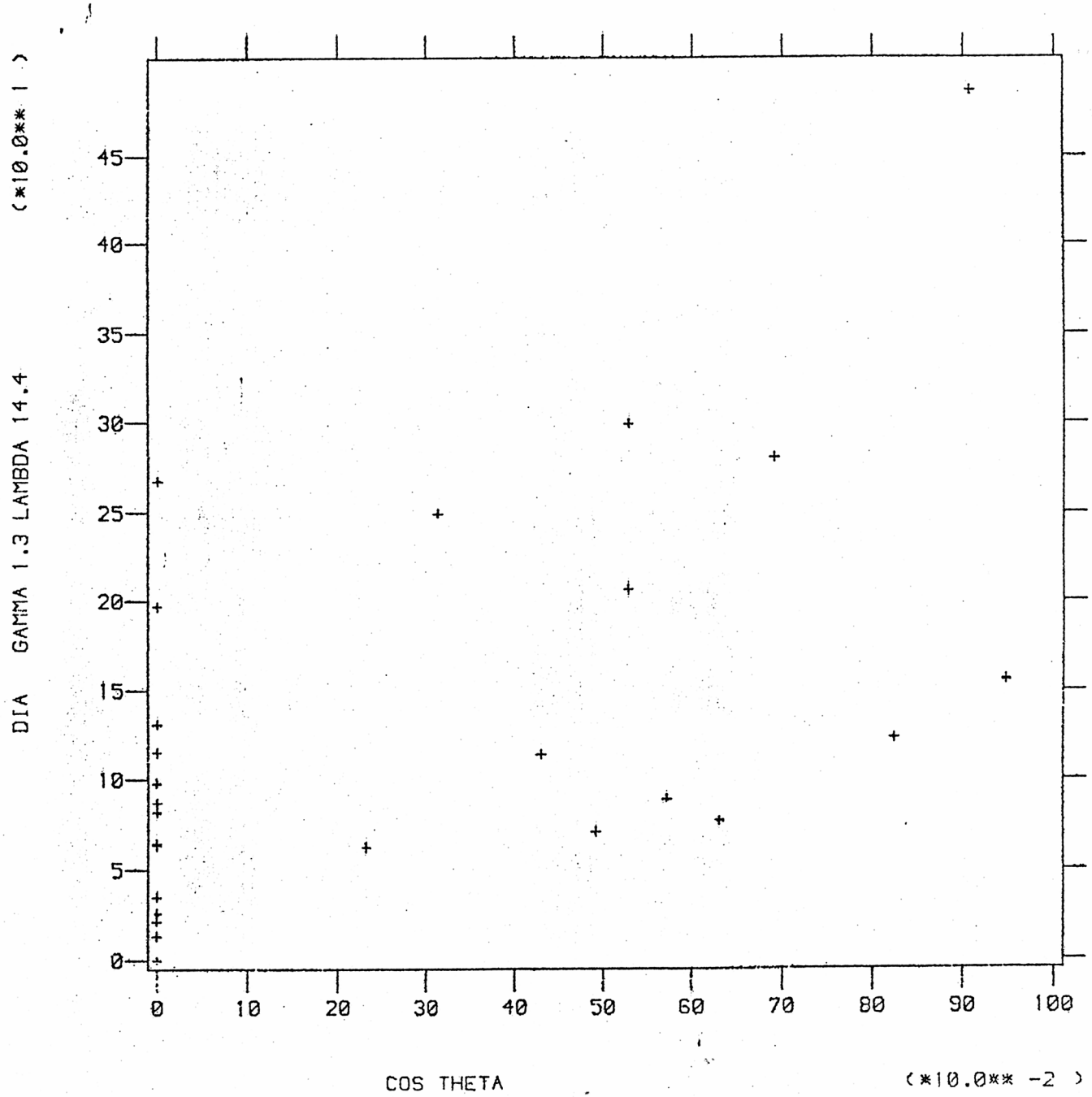
DIA GAMMA 1.3 LAMBDA 14.4
(*10.0** 1)
45
40
35
30
25
20
15
10
5
0
0
10
20
30
40
50
60
70
80
90
100
COS THETA
(*10.0** -2)

Fig 9(c)